Human Walking Adaptations to Distal Limb Mass Disturbances: Investigating Biomimetic Performance Objectives

Benjamin John Swilling

B.S., Mechanical Engineering (2001)

Rensselaer Polytechnic Institute

Submitted to the Department of Mechanical Engineering
In Partial Fulfillment of the Requirements for the Degree of
Master of Science in Mechanical Engineering

at the

Massachusetts Institute of Technology

September 2005

The author hereby grants to MIT permission to reproduce and to distribute publicly paper and electronic copies of this thesis document in whole or in part.

Signature of Author _____

$\bigcirc$ **Benjamin John Swilling**
Department of Mechanical Engineering
June 29, 2005

Certified by _____

Hugh Herr
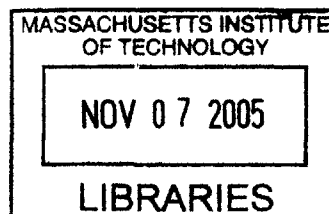Assistant Professor of Media Arts and Sciences
Thesis Supervisor

Certified by _____

/
Lynette Jones
Mechanical Engineering Principle Research Scientist
Thesis Reader

Accepted by _____

Lallit Anand
Chairman, Department Committee on Graduate Students

Human Walking Adaptations to Distal Limb Mass Disturbances: Investigating Biomimetic Performance Objectives

by

Benjamin John Swilling

Submitted to the Department of Mechanical Engineering
In Partial Fulfillment of the Requirements for the Degree of
Master of Science in Mechanical Engineering

Abstract

Online optimal trajectory planning is required in the control of humanoid robots, advanced prostheses, and impaired human limbs via functional neuromuscular stimulation . Optimization problems that involve complex, high degree of freedom simulations of the musculoskeletal system require extensive computational effort to solve. A methodology for generating optimal gait patterns in an online and computationally efficient manner is needed. It is the goal of this thesis to work towards the development of biologic performance criteria that can be utilized in finding solutions to reduced order walking optimization problems.

Toward the development of biologically realistic performance criteria, human subjects were inertially-perturbed and the reorganization of gait quantitatively measured. Ten subjects walked at a self-selected speed with and without a 5 kg mass attached to the right ankle. Kinetic and kinematic data were collected for the weighted and unweighted conditions using ground force platforms and a multi-camera infrared tracking system, respectively. A 16 segment model of the body was built for each subject and a variety of kinematic, kinetic, and total system parameters calculated throughout the gait cycle. Additionally, the normal kinematic dataset was analyzed with a 5 kg mass virtually placed on the right ankle. The virtual mass dataset served as a known suboptimal solution as a basis for comparison.

A Wilcoxon rank sign test was performed, and the ankle-weighted dataset was compared to normal. There were no significant changes in stride frequency, step length, stride length, or self-selected walking speed between the weighted and unweighted walking conditions. There were significant deviations in the kinematics of the right leg, but most were generally small with the exception of a decrease in maximum flexion angle of the affected leg during swing. In comparison to the virtual mass case to the true weighted case, it was determined that the reorganization of gait yields an increase in gait efficiency, a decrease in work to move the body center of mass, and a general reduction in reaction torque of the affected leg. It is suggested that the biologic performance objective consists of some function comprising of the energetic costs to move the body center of mass, gait efficiency, and joint reaction torques.

Hugh Herr
Assistant Professor of Media Arts and Sciences
Thesis Supervisor

Acknowledgements

I'd like to thank everyone who helped me along my way to getting my degree and writing my thesis:

- Dr. Hugh Herr for advising me and really making this work possible.
- Dr. Marko Popovic for always having an open door to listen to my questions.
- Dr. Lynette Jones for acting as my thesis reader and your helpful feedback.
- The Spaulding Gait Lab for their excellent work in taking the data.
- All the members of the Biomechatronics Group/Leg Lab for your help and thesis commiseration.
- My parents William and Deanna for all your love and support and for raising me to aspire to excellence.
- My siblings Emily and Nathan and his wife Jill for your advice and helping me to get my mind away from the lab when I needed it.
- Ruthie Ma for your support and for helping me to stay vigilant during my most trying times.
- All the members of my small group at Park Street Church: Kim M., Kim H., Chris, Mike, Laurie, Sarah, David, Christine, Christina, Debbie, Sue, Karen, and Ben.
- The 2004 Boston Red Sox, while it seemed it took 86 years for me to finish this thesis, yours was still the greater challenge.

Table of Contents

List of Figures

List of Tables

1 Introduction

Walking is a complex process involving the interaction of the neuromuscular system with the ground in a cyclical manner. Giovanni Alfonso Borelli, widely known as the "father of biomechanics", described gait in 1681 in *De Motu Animalium* as: "During walking the human body is always in contact with the ground, supported alternately by one leg and the other. During this alternate support it seems that each half of the body weight is in turn raised and moved." Many applications require the generation of biologically realistic walking patterns, ranging from the control of modern humanoid robots to advanced prostheses and orthoses for the physically challenged. It is generally believed that the human motor control system seeks to optimize some performance criterion during steady state walking (Nubar & Contini 1961, Beckett & Chang 1968, Chow & Jacobson 1971, Hatze 1976, Chou et al. 1995). Synthesis of biologically realistic target trajectories typically requires solving a numerically intensive optimization problem. Solving the walking optimization problem can involve complex simulations of the nonlinear dynamics of human musculature and morphology, involving extensive computational power and time (Anderson & Pandy 1999). In the context of limb prosthetic or orthotic control, it is not currently practical to use such complex methods to generate target trajectories in an online and on demand fashion. A computationally tractable optimization strategy is required until a brain-machine interface

can be devised for direct prosthesis control, or computing technology has progressed to allow rapid online solutions to high-level optimizations.

Anderson and Pandy (2001) postulated that the goal of human movement control is to minimize the metabolic energy per unit distance traveled. By employing a complex simulation consisting of 54 Hill-type musculotendon units and a 23 degree of freedom musculoskeletal model, they were able to predict human walking kinematic data qualitatively. However, the forward dynamics optimization problem was solved using several multiple instruction multiple data parallel computers at the NASA-Ames research center. Anderson and Pandy (1999) used the same model to optimize human vertical jumping, and the convergence of the solution took more than 1800 hours (2.5 months) on a 180 MHz Silicon Graphics machine. The use of a super computer still required nearly 23 hours computation time. While computers are more powerful today than in 1999, the on-board processing capability available today for humanoid robotics or advanced prostheses is far less than that of a super computer, and the required computation time would be far too long. Thus, a reduced order method of generating optimal gait patterns in an online and computationally efficient manner is needed. It is the goal of this thesis to work towards the development of biologic performance criteria that can be utilized in finding solutions to reduced order walking optimization problems.

Human load carrying capability has been studied extensively. However, most of the research has been geared toward evaluating the load carrying abilities of humans with the load transported in a conventional manner, i.e. on the back, head, or symmetrically with the hands, and not geared toward suggesting biological performance objectives for gait (Soule 1969, Givoni 1971, Kamon 1973, Keren et al. 1981, Miller 1987, Graves et al. 1988, Claremont 1988, Cavanagh and Kram 1989, Holt 1990, Bonnard 1991, Knapik 1996, Abe 2004). Holt et al. (2003) placed a backpack containing 40% body weight on the back and found an increase in the effective stiffness of the lower legs so that the amplitude of the vertical excursions of the body center of mass was not significantly altered from normal unweighted walking. This work suggests that the motion of the body center of mass may be a highly regulated quantity and could be invariant to inertial disturbances. Asymmetrical distal loading of healthy subjects has been studied, although not extensively. Skinner and Barrack (1990) placed small loads asymmetrically on the ankles and examined changes in the percentage of stance phase of gait as well as increases in metabolic rate. Donker (2002) placed small loads on the ankle and wrist and noted a general reorganization of physical body segments due to the

added mass to examine the degree to which the body can be modeled as a force driven harmonic oscillator. The goal of the previous papers on asymmetrical mass disturbances was not to generate biologic performance criteria, and thus is of marginal value for this analysis. I hypothesize that there are invariant tendencies in the amplitude and root mean square deviations of the motion of the body center of mass when the human body is inertially perturbed due to the regulation of the body center of mass by the motor control system.

Gu (2003) found when studying the system angular momentum of normal walking that total spin angular momentum and net external moment are low, suggesting that body spin is a strongly regulated quantity in human walking. Furthermore, it was found in the sagittal and transverse planes that body segments move in a fashion so that the vector sum of all their respective spins about the body center of mass is nearly zero. Popovic et al. (2004) found the angular momentum of all body segments can be comprised of three angular momentum primitives in each plane, used this information in an optimization methodology, and generated kinematic joint trajectories that were in qualitative agreement to human kinematic joint data. The work on angular momentum regulation in walking suggests that total angular momentum or net external moment may be a chief component of the biologic performance criterion. I hypothesize that the reorganization of gait due to the inertial disturbance induced, in comparison of the adaptive and non-adaptive weighted cases, a decrease in total angular momentum and net external torque.

A significant property of human walking is that the self-selected speed occurs at the minimum of the gait efficiency versus walking speed curve (Bard & Ralston 1959). The motor control system, at least in some higher level functions such as speed of ambulation, appears to be optimizing to reduce the metabolic demands of walking. Inman (1967) found that the body center of mass follows approximately a sinusoidal pattern, and that this is the most efficient type of movement due to the cyclical conversion of body center of mass energy from gravitational potential energy into kinetic energy. Nubar and Contini (1961) and Chow and Jacobson (1971) suggested that the human motor control system regulates movement in a manner that minimizes muscular effort, calculated by the sum of the squares of joint torques. Beckett and Chang (1968) hypothesized that optimal gait patterns can be synthesized by minimizing the amount of mechanical work done to move the body. Chou et al. (1995) examined movement of the swing leg, and found that reducing the mechanical energy required to move the leg

provided results that were generally similar to experimental gait data. I hypothesize that adaptations of gait due to the inertial disturbance yielded a reduction of the energetic costs of moving the body center of mass, increased movement efficiency of the body center of mass, and reduced joint reaction torques.

With the goal of developing biologically realistic performance criteria for use with reduced order models, human subjects were asymmetrically inertially perturbed and the reorganization of gait quantitatively measured. Subjects were asymmetrically distally loaded because it was assumed the greater distance from the body center of mass of the load and the resultant asymmetry of gait would simplify the investigation into the biologic performance objectives. Using the motion laboratory at Spaulding Rehabilitation Hospital, kinematic walking data was taken with an eight camera infrared motion capture system. Walking kinematics were recorded for two loading conditions: unloaded normal walking and weighted walking with a five kilogram mass on the right shin. Both walking trials were performed at a regulated self-selected normal walking speed for consistency. The reorganization of gait due to the inertial disturbance was quantified using two chief comparisons. Normal walking data was compared to the adapted weighted data to search for invariant qualities of gait. Secondly, a non-adaptive weighted case was synthesized by recalculating the dynamics of normal walking with a 5 kg mass virtually placed on the right shin and compared to the adaptive weighted case. It was assumed that the dynamics of the non-adaptive weighted case served as a biologic "starting point", and thus all biologic adaptations were an effort to minimize the biologic cost function. A variety of gait parameters calculated from joint reaction torques, joint kinematics, and total system dynamics were defined and statistically significant deviations of these parameters identified.

In order to clarify the constitution of a cost criterion for human walking, gait data were collected for healthy subjects ambulating with and without masses placed distally on the shin. The reorganization of walking due to the added mass was quantitatively defined by nonparametric statistical comparison to normal unweighted walking. I hypothesize that the induced changes of gait due to the added mass in comparison of the adaptive and non-adaptive datasets were a reduction of the energetic costs to move the body center of mass and an increase of the energetic efficiency of the body center of mass motion. Furthermore, I hypothesize that the adaptations of gait decreased system angular momentum and net external torque, and there are invariant tendencies in the motion of the body center of mass. Finally I hypothesize that the reorganization of gait

yielded, in comparison of the adaptive and non-adaptive datasets, a decrease in joint reaction torques, and that the adaptive changes in gait were manifested by significant deviations in joint kinematics. These hypotheses were tested by evaluation of a number of kinematic, kinetic, and total system gait parameters.

1.1   Motivation

The motivation for this thesis is to provide the groundwork for biomimetic control of prostheses, humanoid robotics, and functional neuromuscular stimulation (FNS) of muscles. Until a brain-machine interface can be utilized for direct control in the case of prosthetic control or FNS, it will be necessary to supplement basic user intent recognition with a high-level, biologically-realistic controller. There may be restrictions in the control of a prosthesis or humanoid robot that could be accounted for by adding constraints to the biological optimization problem. For example, in the control of a semi-active knee prosthesis where the controllable element is a variable damper, it would be possible to predict a target gait with the constraint that the prosthetic knee can only dissipate power. Thus, instead of targeting a fixed trajectory, kinematic target trajectories could rapidly be generated online that adjust to changes in terrain, walking, speed, and morphology.

1.2   Contribution

This thesis focuses on elucidating elements in the performance criterion that the motor control system optimizes during walking. This work can be used in areas from powered prosthetic control to functional neural stimulation and humanoid robotics. Understanding the mechanisms by which the motor control system controls the body during walking will allow better understanding of gait and further interfusion of man and machine to aid the rehabilitation of physically challenged individuals.

1.3   Thesis Outline

Chapter 2 presents some basic biomechanical terms and an overview of the function of the ankle, knee, and hip during the gait cycle. Chapter 3 describes the experimental methods and the numerical analyses performed. Chapter 4 presents the results of the analyses. Chapter 5 contains discussion regarding the results, general conclusions, and recommendations for future work.

2   Background

This chapter details some general information commonly used in the study of human gait. Section 2.1 describes the gait cycle in detail and the behavior of thigh, knee, and ankle during walking.

2.1   The Gait Cycle

The gait cycle begins when the heel of the right foot strikes the ground, and ends with the succeeding contact of the right heel with the floor. There are four distinct support phases through the gait cycle (Sutherland 1988). When the gait cycle begins, both the right and left foot are in contact with the floor; this is the first period of double support. Roughly 10% through the gait cycle, the left foot lifts off the ground and the left leg enters swing, this is the right leg single support phase. At the commencement of left leg swing halfway through the gait cycle, the left heel strikes the ground, beginning the second period of double support. At an average of 60% through the gait cycle the right leg enters swing, this begins the left leg single support phase. The right leg is in swing for the remaining 40% of the gait cycle, and the next gait cycle begins at ground contact of the right foot at the termination of right leg swing.
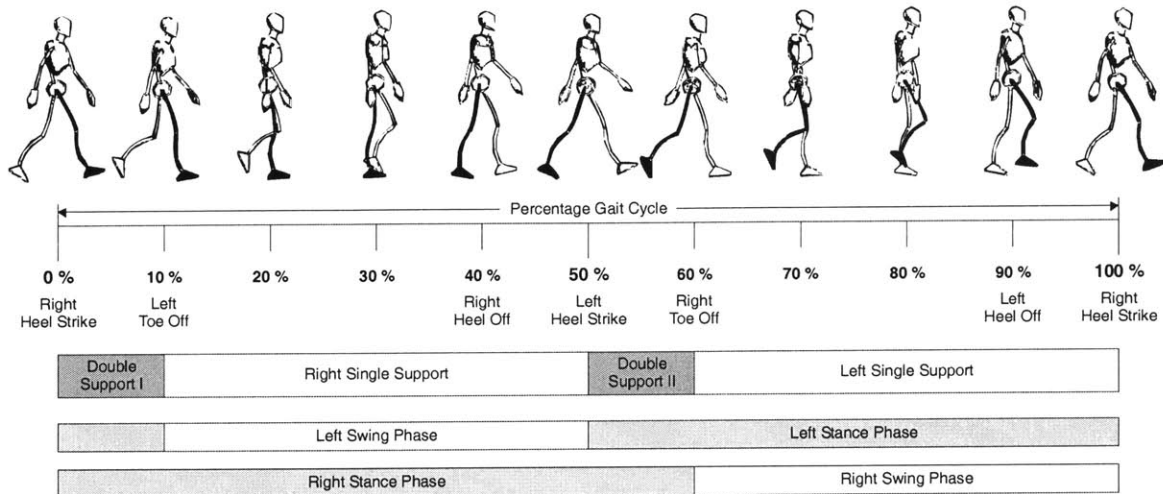
Figure 2.1.1 The Gait Cycle. The black leg of the walking stick-man is the right leg. A gait cycle is measured in percentage and is defined by consecutive ground contacts of the right foot. Adapted from Inman et al. (1981)

The gait cycle has been partitioned into discrete phases a number of times (Perry 1992, Sutherland 1988, Winter 1990). In this thesis the Perry gait definitions were used in examination of torques and powers about the joints of the lower leg and peak kinematics. Similar to the gait cycle defined above, the Perry gait cycle is defined by consecutive contacts of the right heel with the ground. The stance phase is divided into four phases: loading response, mid-stance, terminal stance, and pre-swing. The loading response describes the transfer of load from the upper body from the left leg to the right leg. The loading response ends as the left foot lifts off the ground and mid-stance begins. During the loading response the direction of the body center of mass is redirected from a downward direction to an upward direction (Inman et al. 1981). Mid-stance ends as the body center of mass passes over the right foot and begins to descend preparing for contact of the left foot. Terminal stance is the period after mid-stance at which the body center of mass is forward of the support foot and ends when the knee reaches its maximum stance extension and the left heel makes contact with the ground. Pre-swing describes the period of stance after terminal stance where the knee is flexing rapidly as the load transfers from the right leg to the left leg and it terminates when the right toe loses contact with the ground. The swing phase of gait is partitioned into three phases: initial swing, mid-swing, and terminal swing. Initial swing begins at toe-off and terminates when the knee becomes maximally flexed. Mid-swing begins at the maximal flexion point of the knee and continues until the sagittal projection of the tibia is parallel to the vertical axis. During mid-swing the behavior of the shank is mostly

pendular as torque about the knee is very low. The last phase of swing begins after the termination of mid-swing and ends when the right foot makes contact with the floor once again.

	Phase of Gait	Begins	Ends
Stance	Loading Response	Initial Contact	Contralateral toe off
	Mid-Stance	Contralateral toe off	BCM proceeds forward of the support foot
	Terminal Stance	BCM proceeds forward of the support foot	Contralateral heel strike
	Pre-Swing	Contralateral heel strike	Toe off
Swing	Initial Swing	Toe off	Maximum knee flexion
	Mid-Swing	Maximum knee flexion	Tibia parallel to vertical axis
	Terminal Swing	Tibia parallel to vertical axis	Initial contact

Table 2.1.1 Perry's definition of the phases of gait.
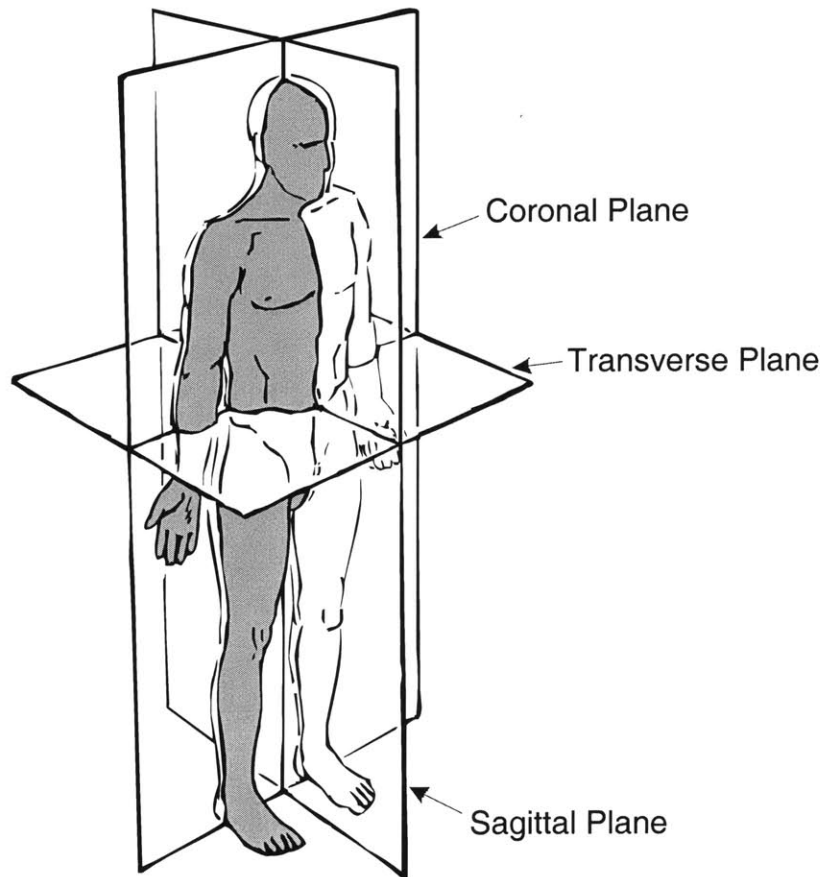
Figure 2.1.2 The three principle planes of the body, from Inman et al. (1981).

2.1.1   Ankle Function during the Gait Cycle

Most of the activity at the ankle occurs during the stance phase. The main goal of the ankle during swing is to dorsiflex enough so that the toe has sufficient clearance with the ground to prevent stumbling. At heel strike the ankle is near its neutral position, and during the loading response it enters controlled plantarflexion (Whittle 1996). Plantarflexion of the ankle brings the foot from the heel rocker position at initial contact to foot flat. A dorsiflexor moment about the ankle during the loading response results in a small negative power due to eccentric contraction of the tibialis anterior. Loss of function of the tibialis anterior muscle results in the condition known as drop foot where the foot slaps on the ground during loading response (Blaya 2003). After foot-flat the direction of the moment about the ankle changes from dorsiflexor to plantarflexor and the tibialis anterior ceases to contract and is replaced by eccentric contraction of the triceps surae. The ankle continues to dorsiflex through mid- and terminal stance with an internal plantarflexor torque resisting this movement causing power absorption. During pre-swing the ankle goes into powered plantarflexion mode causing the largest positive power peak throughout the gait cycle. The peak plantarflexor torque occurs just about at the transition from terminal stance to pre-swing. Just after toe-off the ankle reaches its maximum plantarflexed position. The contraction of the triceps surae ceases and the tibialis anterior contracts again to dorsiflex the ankle for swing. Since the foot is no longer in contact with the ground, torque is only needed to accelerate the inertia of the foot. Given the relatively small mass of the foot compared to the body, torques and powers at the ankle during swing are marginal in comparison to the rest of the gait cycle (see Figure 2.1.3). During mid-swing the ankle moves from a plantarflexed position back to a neutral position to prepare for heel-strike.

Figure 2.1.3 Ankle function during the gait cycle. Ankle angle, torque about the principle axis of rotation, and joint power for a 65.3 kg 35 year old female at self-selected walking speed are shown. Torque and power has been normalized for body weight.

2.1.2   Knee Function during the Gait Cycle

At the start of the gait cycle, at initial contact, the knee is flexed anywhere from 2-5º from late swing retraction. During the loading response the knee flexes to a maximum of roughly 15-20º (see Figure 2.1.4). There is an internal extensor moment about the knee provided by eccentric contraction of the quadriceps. The extensor moment about the knee limits the speed and magnitude of knee flexion during stance (Whittle 1996). During the loading response the muscle activity about the knee is predominantly dissipative. The knee reaches its maximal point of flexion during mid-stance and starts to extend afterwards. The quadriceps muscles contract eccentrically and then concentrically as the knee passes from flexion to extension. Stance extension

requires positive power and this is the reason why semi-passive or totally passive knee prostheses can not provide proper stance flexion because they do not have the capability for powered stance extension. During terminal stance the knee becomes maximally extended. The ankle, reaching its maximum dorsiflexed position during terminal stance, soon enters powered plantarflexion. The center of pressure of the ground reaction force by this time has moved to the fore-foot and would tend to cause a hyperextension of the knee. The gastrocnemius muscle contracts providing an internal flexor moment about the knee and limits the amount of knee extension. The ground reaction force vector is directed so that it tends to flex the knee as the knee enters pre-swing. This external knee flexor is counteracted by eccentric contraction of the rectus femoris to limit the amount of knee flexion. At toe-off the knee has reached roughly half of its maximal flexion; most of the behavior of the knee during swing is due to the natural pendular behavior of the leg during swing (Anderson et al. 2004). There is a small internal flexor moment to limit the flexion of the knee. During mid-swing as the knee reaches its maximally flexed position, the hamstrings contract eccentrically to limit the speed of swing extension. During terminal swing, the knee becomes maximally extended and flexes slightly during late swing retraction. Late swing retraction reduces the peak impact loads during initial contact and subsequently reduces the amount of energy lost during the initial ground impact (Winter 1992).
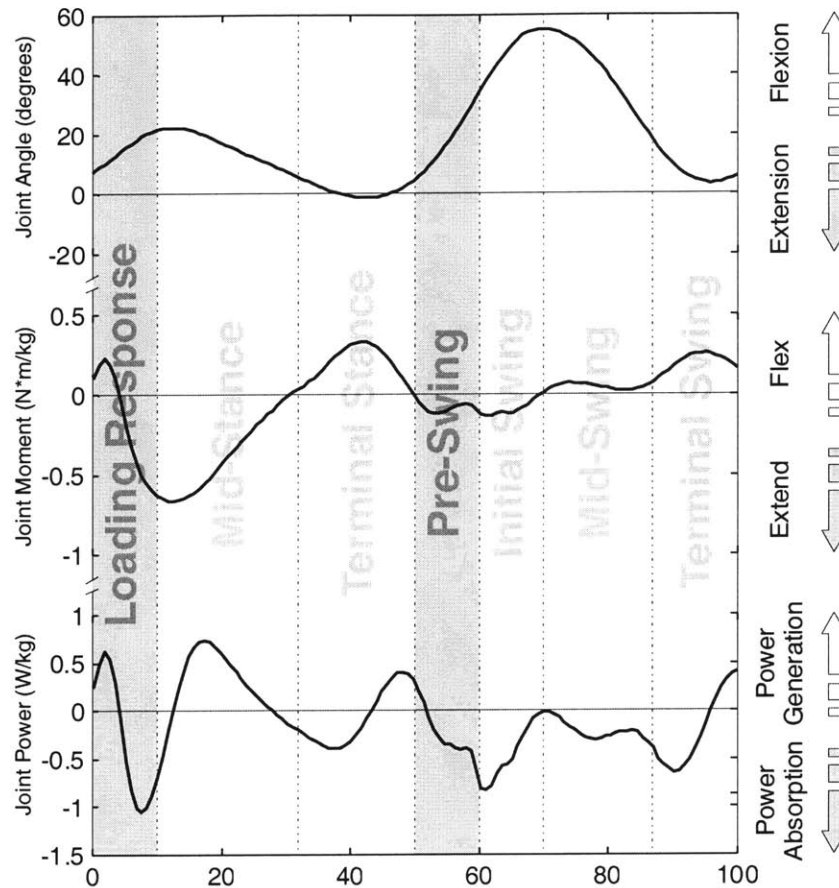
Figure 2.1.4 Knee function during the gait cycle. Knee angle, torque about the principle axis of rotation, and joint power for a 65.3 kg 35 year old female at self-selected walking speed are shown. Torque and power has been normalized for body weight.

2.1.3   Hip Function during the Gait Cycle

The thigh reaches a point of maximal flexion during swing and its angle does not change much until initial contact. The gluteus maximus and hamstring muscles contract concentrically during the loading response creating an extensor moment which causes the thigh to start to extend. During mid-stance the knee passes from flexion into extension. The internal extensor moment declines then ceases all together when the concentric contraction of the gluteus maximus and hamstrings stops. Near the change from mid-stance to terminal stance the moment about the hip changes from an extensor moment to a flexor moment and subsequently the power flow goes from generation to absorption. The thigh becomes maximally extended at the entrance to pre-swing and

contralateral leg initial contact. Also at this point the largest hip flexor is seen, due predominantly to the contraction of the adductor longus and the rectus femoris muscles which results in flexion of the thigh (see Figure 2.1.5). During pre-swing and initial swing there is a powerful contraction of the iliopsoas to provide an impulse of power to the swing leg (Whittle 1996). In the initial swing phase the point of maximum positive power transfer at the hip occurs. During mid-swing the hip reaches a point of roughly maximum flexion and then maintains its orientation through terminal swing. There is a large torque generated about the hip during terminal swing as the knee goes into swing extension. Although the torque magnitude is large, the hip is roughly static so that power absorption is very small. The torque about the hip allows the transfer of kinetic energy from the swing shank and foot to the trunk (Siegel et al. 2004).
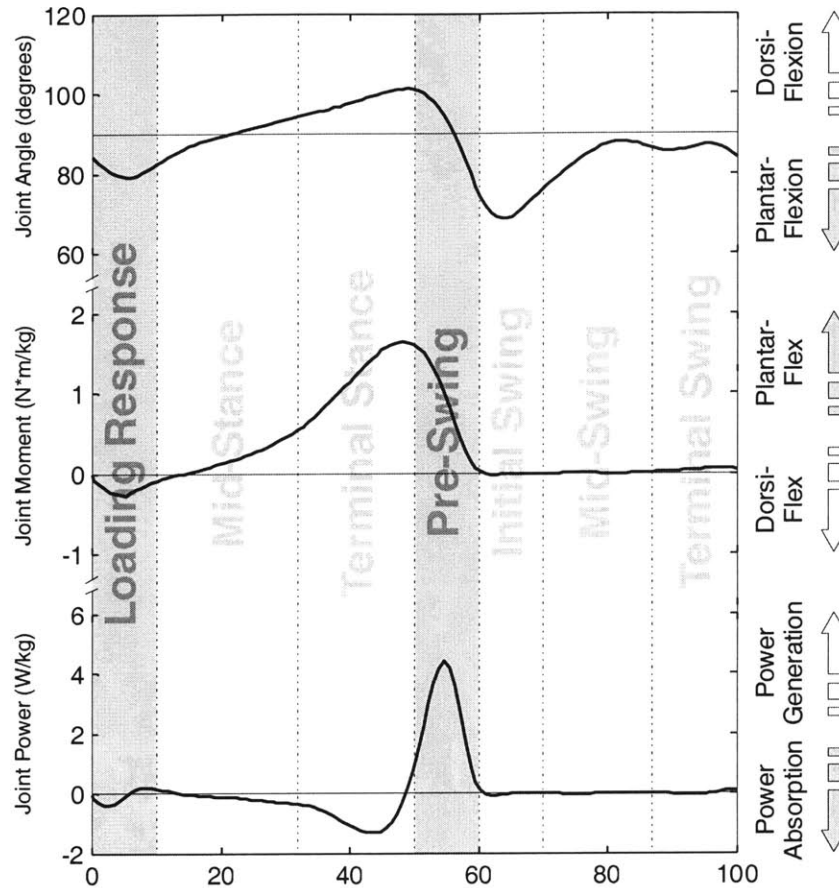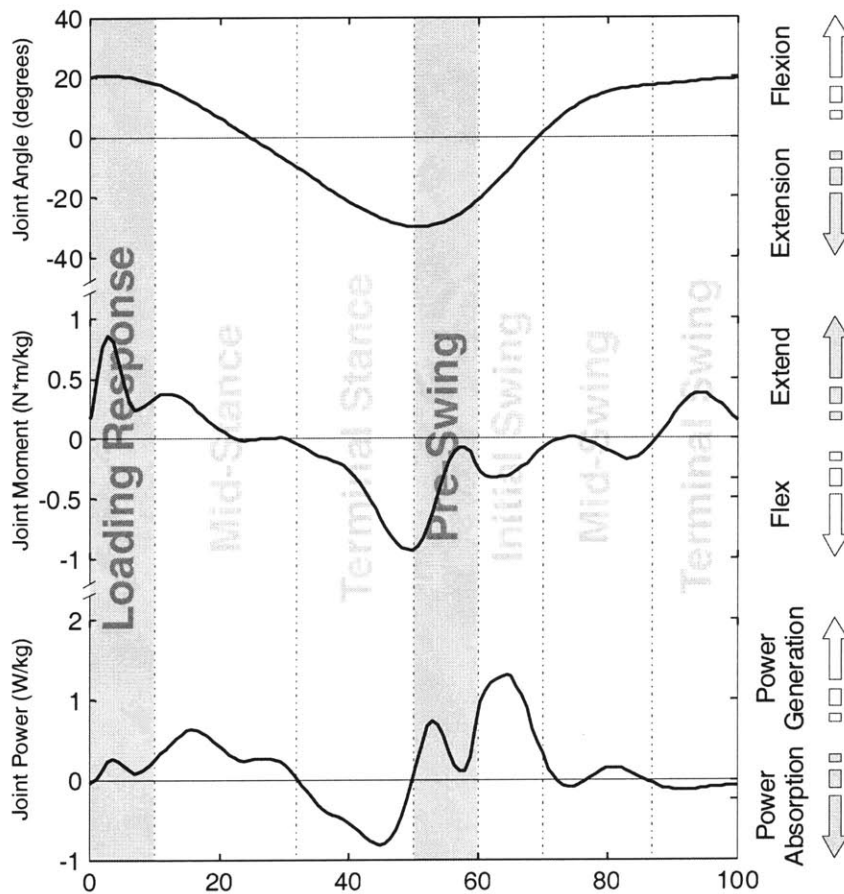

Figure 2.1.5 Hip function during the gait cycle. Hip angle, torque about the principle axis of rotation, and joint power for a 65.3 kg 35 year old female at self-selected walking speed are shown. Torque and power has been normalized for body weight.

3 Materials and Methods

This chapter outlines the experimental procedures and numerical methods used in this thesis. Section 3.1 describes the 10 subjects from whom kinematic marker location and ground reaction force data were taken. Section 3.2 and 3.3 describe the laboratory instrumentation and experimental protocol. In section 3.4 the initial data processing steps are discussed, followed by section 3.5 in which the methods for determining gait events, e.g. heel strike, are described. Section 3.6 provides a more in-depth description of the modeling techniques used for modeling the human body. Section 3.7 describes the nonparametric statistical methods used for pair wise comparisons between the data. Finally, section 3.8 defines some of the gait parameters compared in chapter 4.

3.1 Participants

3.1.1 Subject Anthropometric Data

Ten able-bodied subjects participated in this study. The participants consisted of five men and five women. The mean age of the men was 28 while their mean weight was 76.1 kg and their mean height was 1.84 m. The mean age of was 23 and their

mean weight was 56.9 kg while their mean height was 1.67 m. Subjects had no known neurological or physiological impairments that could have affected their gait. Subjects recruited were friends, family, and coworkers of the principal investigator. In compliance with MIT policies, this study was conducted according to guidelines provided by the Committee On the Use of Humans as Experimental Subjects at MIT. Subject anthropometric data were taken in accordance with common lab practices.

Subject Number	Age	Mass (kg)	Height (m)	Foot Length (m)	Shin Length (m)	Thigh Length (m)	Hand Length (m)	Forearm Length (m)	Upper Arm Length (m)	Sex
1	31	76.8	1.85	0.240	0.476	0.414	0.160	0.272	0.247	Male
2	27	81.9	1.87	0.273	0.471	0.431	0.216	0.290	0.246	Male
3	22	73.9	1.82	0.300	0.450	0.420	0.200	0.286	0.241	Male
4	33	64.6	1.79	0.250	0.451	0.389	0.195	0.259	0.260	Female
5	21	62.7	1.69	0.225	0.390	0.394	0.185	0.263	0.246	Female
6	36	65.3	1.76	0.270	0.447	0.389	0.190	0.281	0.240	Male
7	24	82.6	1.92	0.280	0.458	0.447	0.210	0.292	0.248	Male
8	21	49.9	1.60	0.230	0.373	0.365	0.180	0.247	0.223	Female
9	21	50.1	1.58	0.235	0.366	0.391	0.170	0.240	0.229	Female
10	21	57.2	1.67	0.250	0.374	0.407	0.180	0.245	0.226	Female

Table 3.1.1 Subjects' mass, height, measured anthropometric data, and sex.

Measurement	Methodology
Height	Distance from the floor to the most cranial point on the head.
Shin Length	Distance from the knee joint center to lateral malleolus.
Foot Length	Distance between calcaneus and acropodion.
Thigh Length	Distance between the trochanterion and the knee joint center.
Hand Length	Distance between the wrist joint center and the third dactylion.
Forearm Length	Distance between the elbow joint center and wrist joint center.
Upper Arm Length	Distance between the shoulder joint center and the elbow joint center.

Table 3.1.2 Anthropometric measurement methodology.
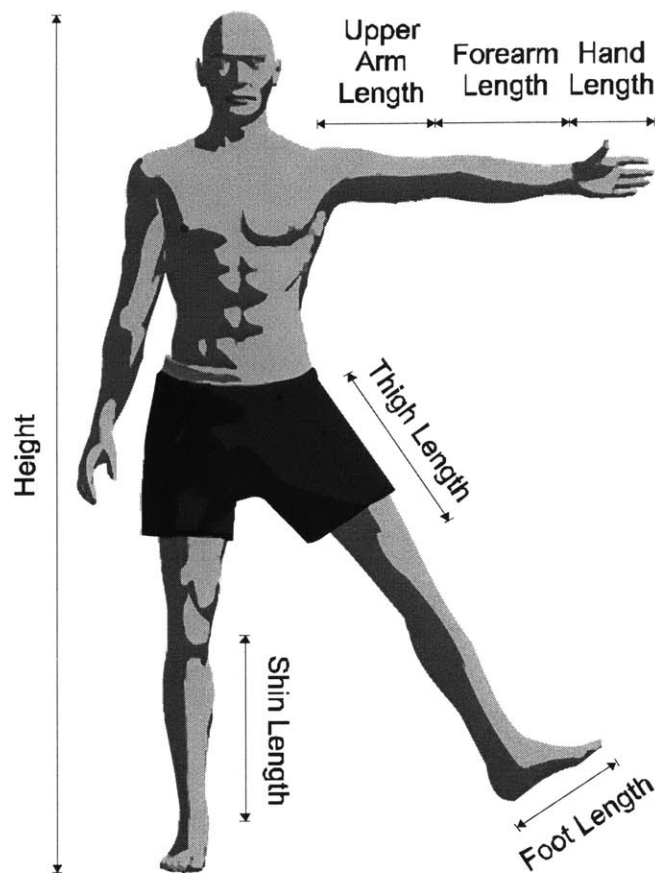
Figure 3.1.1 Subject measurements.

3.1.2   Supplemental Anthropometric Data

The subject measurements taken prior to testing were insufficient to build a realistic model of the body. These measurements needed to be supplemented with estimated anthropometric measurements based upon published data. Data from de Leva (1995) and Tilley (2001) were used to supplement the direct subject measurements.

Table 3.1.3 Supplemental anthropometric data from literature.

Measurement	Endpoints	Methodology Male	Methodology Female
Trochanterion Height	Distance from the floor to the trochanterion	$0.0463^{a}*H + l_{shin} + l_{thigh}$	$0.0453^{a}*H + l_{shin} + l_{thigh}$
Trunk and Head Length	Vertex to trochanterion	$H - l_{trochanterion\ height}$	
Head Length	Vertex to cervicale	$0.1395*H$	$0.1405*H$
Trunk Length	Cervicale to trochanterion	$l_{trunk\ and\ head\ length} - l_{head\ length}$	
Pelvis Length	Mid-hips to omphalion	$0.2402*l_{trunk\ length}$	$0.2936*l_{trunk\ length}$
Abdomen Length	Omphalion to substernale	$0.3553*l_{trunk\ length}$	$0.3324*l_{trunk\ length}$
Chest Length	Substernale to cervicale	$0.3992*l_{trunk\ length}$	$0.3692*l_{trunk\ length}$
Cervicale to Sternum	Cervicale to suprasternale	$0.1177*l_{trunk\ length}$	$0.1384*l_{trunk\ length}$

a Tilley 2001
All other data from de Leva 1995
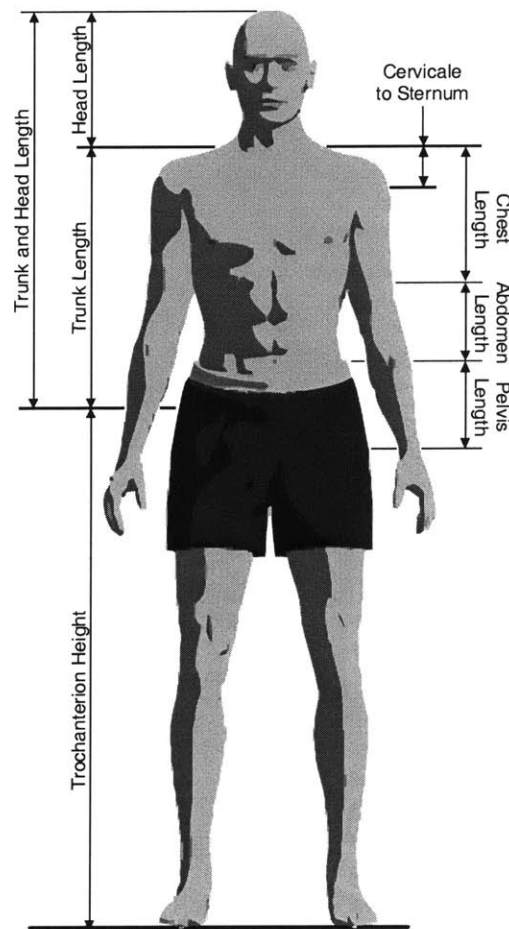
Figure 3.1.2 Supplemental anthropometric measurements taken from literature.

3.2   Instrumentation

All subject testing was performed at the Motion Laboratory in the Spaulding Rehabilitation Hospital located in Boston, Massachusetts. Three-dimensional kinematic data were recorded using an eight camera infrared Vicon motion capture system (VICON 512, Oxford Metrics, Oxford, UK) at a sampling rate of 120 Hz. Ehara et al. (1997) found a less capable six camera VICON 370 system had a mean absolute marker location error of 0.94 mm. Reflective markers were placed on bony landmarks on the subject's body using a Plug-in-Gait marker set: sixteen lower body markers, five trunk markers, eight upper limb markers, and four head markers. Ground reaction force data were acquired from two AMTI force-plates (Watertown, MA) at 1080 Hz. Force-plate data was resampled down to 120 Hz when used in the analyses.
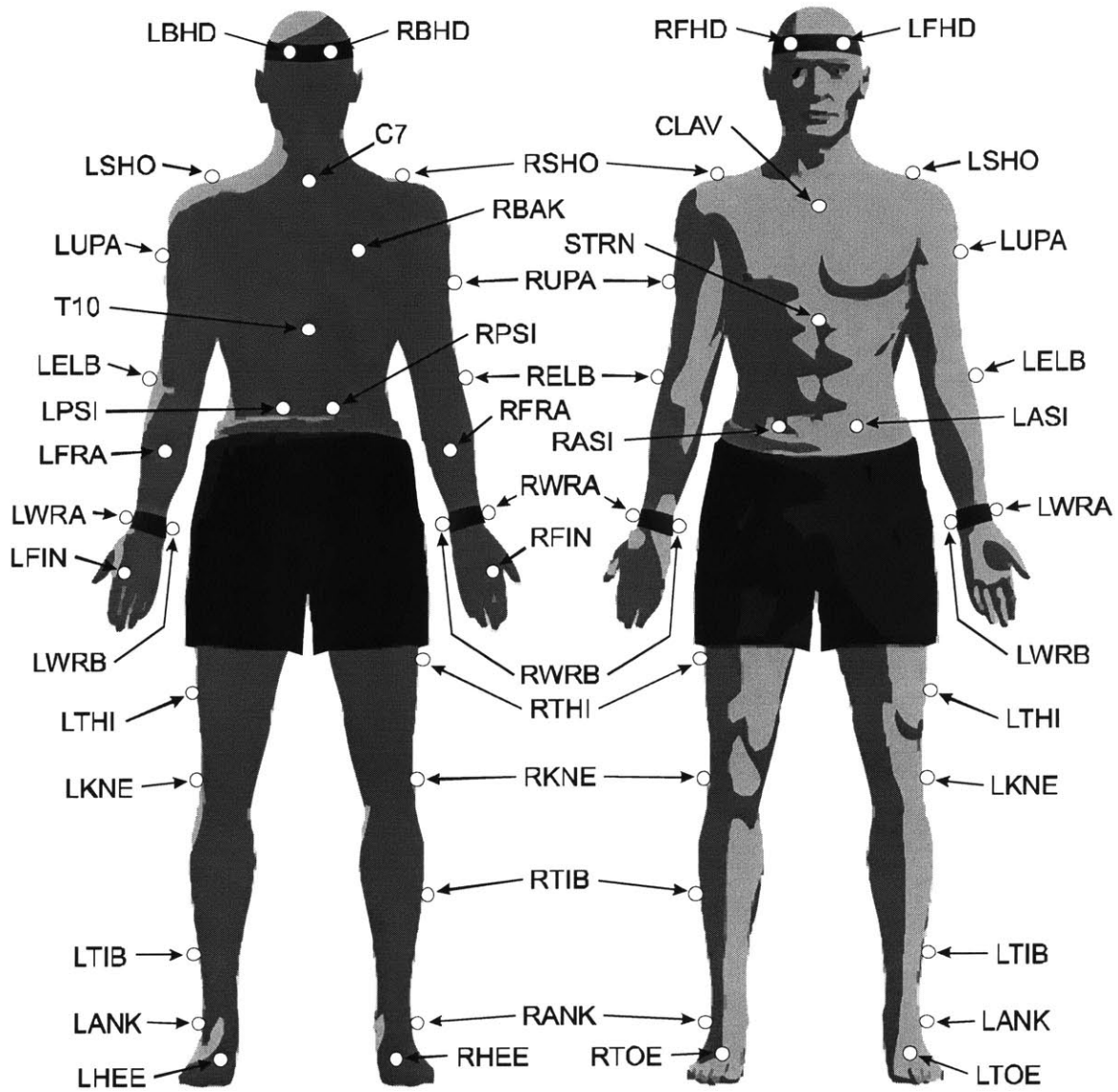
Figure 3.2.1 Reflective marker placement for Vicon 512 motion capture system. Marker definitions are provided in Table 3.2.1

Marker Name	Description	Placement
LFHD	Left front head	Located approximately over the temple.
RFHD	Right front head	
LBHD	Left back head	Back of the head at a constant height above the floor.
RBHD	Right back head	
C7	Back of neck	Spinous process of the 7th cervical vertebrae.
T10	Upper back	Spinous process of the 10th thoracic vertebrae.
CLAV	Clavicle	Jugular notch where the clavicles join the sternum.
STRN	Bottom of sternum	Xiphoid proces of the sternum.
RBAK	Right upper back	Middle of the right scapula.
LSHO	Left shoulder	Placed on the acromioclavicular joint.
RSHO	Right Shoulder	
LUPA	Left upper arm	Placed on the upper arm between the elbow and shoulder.
RUPA	Right upper arm	
LELB	Left elbow	Located on the lateral epicondyle.
RELB	Right elbow	
LFRA	Left forearm	Placed on the forearm between the elbow and wrist.
RFRA	Right forearm	
LWRA	Left wrist A	Wrist bar, thumb side
RWRA	Right wrist A	
LWRB	Left wrist B	Wrist bar, little finger side
RWRB	Right wrist B	
LFIN	Left finger	Located just below the head of the 2nd metacarpal.
RFIN	Right finger	
LASI	Left ASIS	Placed over the anterior superior iliac spine.
RASI	Right ASIS	
LPSI	Left PSIS	Placed over the posterior superior iliac spine.
RPSI	Right PSIS	
LTHI	Left thigh	Located over the lateral surface of thigh.
RTHI	Right thigh	
LKNE	Left knee	Placed on the lateral epicondyle of the knee.
RKNE	Right knee	
LTIB	Left tibial marker	Placed over the lower lateral surface of the shank.
RTIB	Right tibial marker	
LANK	Left ankle	Located on the lateral malleolus.
RANK	Right ankle	
LHEE	Left Heel	Located on the calcaneous.
RHEE	Right Heel	
LTOE	Left Toe	Placed on the 2nd metatarsal head.
RTOE	Right Toe	

Table 3.2.1 Plug-in-Gait marker definitions.

The motion capture global coordinate frame is oriented so that forward walking is directed along the positive y-axis, vertical movements along the z-axis, and medio-lateral movements along the x-axis.
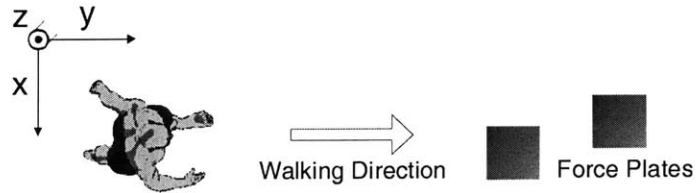
Figure 3.2.2 Configuration of global coordinate frame and force plates in motion laboratory.

3.3   Protocol

All subjects walked barefoot at a self-selected moderate speed over the 10 meter walk-way located at the Spaulding Motion Laboratory. Subjects were timed with a standard stopwatch to ensure the same walking speed over all trials, and trials were subsequently rejected if there was a greater than ± 5% variance in traversal time. After the subject walked along the pathway, the data were quickly analyzed to ensure that the necessary markers were located by the Vicon system and that proper contact was made with both force platforms.

Although only two loading conditions at a self-selected moderate speed are considered in this thesis, initial testing consisted of five loading conditions and two speeds: self-selected moderate and slow. In addition to normal unloaded walking, a 5 kg mass was placed proximally either the left or right wrist and proximally on either the left or right ankle. The order of speeds and walking conditions were randomized in order to mitigate any effects of fatigue. After each change in loading condition the subject was given a brief amount of time to test their gait under the new condition. Only the loaded and right ankle loading conditions at self-selected moderate speed were considered in this thesis. The load placed on the ankle is a considerable distance away from the body center of mass, and thus only the ankle loading data were analyzed because it was assumed the greater distance would have a larger effect on gait and the biologic performance criterion would be more recognizable.

3.4　Initial Data Processing

The three-dimensional kinematic marker location data was first processed with Vicon BodyBuilder (Oxford Metrics, Oxford, UK). Vicon BodyBuilder uses an internal model, in addition to marker location data and measured anthropometric subject data to estimate bone and joint center locations. Kinematic data is first analyzed and any small data gaps are filled with interpolated values, then a Woltring filter (1985) is applied to the data.

3.4.1　The Woltring Filter

The Woltring filter is an optimal filter used commonly in the analysis of motion capture data. Noisy position data is fitted with an optimally regularized natural quintic spline. The benefits to this method are that higher order derivatives can be calculated from the analytic derivative of the polynomial spline, however in this thesis derivatives were found numerically since the Woltring was applied internally within the Vicon software.

3.4.2　Vicon BodyBuilder Bone Models

The kinematic data from the 33 reflective markers were processed in the Motion Laboratory with Vicon BodyBuilder. Using measured anthropometric data from the subject and the marker location data, BodyBuilder uses internal functions to model 13 bones and segments of the body including: clavicle, neck, thorax, humerus, radius, hand, skull, pelvis, sacrum, femur, tibia, foot, and forefoot. The BodyBuilder bone models were used for segment orientations and joint center locations for the hands, forearms, upper arms, feet, shanks, and thighs.
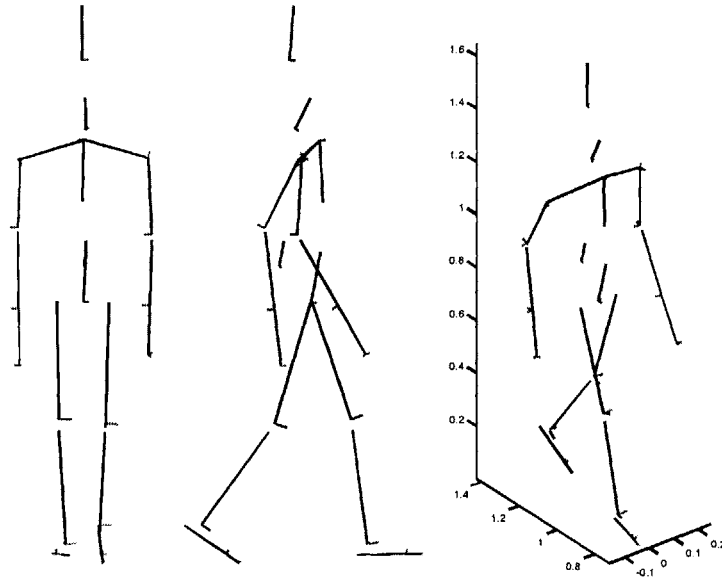
Figure 3.4.1 Vicon BodyBuilder internal bone modeling. Coronal, sagittal, and isometric views are shown.

3.4.3 Coordinate Kinematics and Rotations

3.4.3.1 Coordinate Transformations

In the model of the human body used for this analysis, 16 separate coordinate frames for each of the modeled body segments were used. Each coordinate frame is defined by three orthonormal vectors describing orientation and a three element spatial vector describing the coordinate frame location (Schilling 1990).

Let $\vec{p}$ be a vector in $\Re^3$ and let $X = [\vec{x}_1, \vec{x}_2, \vec{x}_3]$ be an orthonormal set for $\Re^3$, that is: $\vec{x}_1 \cdot \vec{x}_2 = \vec{x}_2 \cdot \vec{x}_3 = \vec{x}_1 \cdot \vec{x}_3 = 0$. Then the coordinates of $\vec{p}$ with respect to X are p^x and are defined by:

$$\vec{p} = \sum_{k=1}^{n} p_k^x \vec{x}_k$$

X is known as a coordinate frame and in the trivial case, the coordinate frame is simply the identity matrix. Where:

$$\bar{p} = [p_i, p_j, p_k]^T \qquad X = \begin{bmatrix} 1 & 0 & 0 \\ 0 & 1 & 0 \\ 0 & 0 & 1 \end{bmatrix} \qquad \bar{p} = p_i \begin{Bmatrix} 1 \\ 0 \\ 0 \end{Bmatrix} + p_j \begin{Bmatrix} 0 \\ 1 \\ 0 \end{Bmatrix} + p_k \begin{Bmatrix} 0 \\ 0 \\ 1 \end{Bmatrix}$$

A rotation matrix is a 3×3 orthonormal matrix that transforms vectors in $\mathfrak{R}^3$ from one coordinate system to another.

3.4.3.2   Fundamental Rotations

If a variable coordinate frame X_{mobile} is obtained from the fixed coordinate frame X_{fixed} by rotating about one of the orthonormal unit vectors of X_{fixed} then the resulting coordinate transformation matrix is a fundamental rotation matrix. In $\mathfrak{R}^3$ there are three possible fundamental rotation matrices defined by a rotation of ψ about the three unit vectors of X_{fixed}.

$$R_x(\psi) = \begin{bmatrix} 1 & 0 & 0 \\ 0 & \cos\psi & -\sin\psi \\ 0 & \sin\psi & \cos\psi \end{bmatrix}$$

$$R_y(\psi) = \begin{bmatrix} \cos\psi & 0 & \sin\psi \\ 0 & 1 & 0 \\ -\sin\psi & 0 & \cos\psi \end{bmatrix}$$

$$R_z(\psi) = \begin{bmatrix} \cos\psi & -\sin\psi & 0 \\ \sin\psi & \cos\psi & 0 \\ 0 & 0 & 1 \end{bmatrix}$$

A combination of three fundamental rotation matrices will allow us to define any rotation matrix R as the composite rotation of three fundamental rotation matrices. This decomposition of R is not unique as there are many possible permutations of fundamental rotations that could be used, i.e. a roll-pitch-yaw versus a yaw-pitch-roll composite rotation.

Once an orientation transformation matrix was found for any particular body segment the 3×3 rotation matrix was stored as a yaw-pitch-roll composite rotation of

$$R = R_z(\theta_3) R_y(\theta_2) R_x(\theta_1).$$

$$R = \begin{bmatrix} \cos\theta_2\cos\theta_3 & \sin\theta_1\sin\theta_2\cos\theta_3 - \cos\theta_1\sin\theta_3 & \cos\theta_1\sin\theta_2\cos\theta_3 + \sin\theta_1\sin\theta_3 \\ \cos\theta_2\sin\theta_3 & \sin\theta_1\sin\theta_2\sin\theta_3 + \cos\theta_1\cos\theta_3 & \cos\theta_1\sin\theta_2\sin\theta_3 - \sin\theta_1\cos\theta_3 \\ -\sin\theta_2 & \sin\theta_1\cos\theta_2 & \cos\theta_1\cos\theta_2 \end{bmatrix}$$

The decomposition of R into a yaw-pitch-roll composite rotation of θ_3, θ_2, and θ_1 is not unique and there will be two sets of angles related by:

$$\theta_1' = \theta_1 + \pi \cdot \left(1 - \operatorname{sgn}\theta_1 - (\operatorname{sgn}\theta_1)^2\right)$$
$$\theta_2' = -\theta_2 + \pi \cdot \left(1 - \operatorname{sgn}\theta_2 - (\operatorname{sgn}\theta_2)^2\right)$$
$$\theta_3' = \theta_3 + \pi \cdot \left(1 - \operatorname{sgn}\theta_3 - (\operatorname{sgn}\theta_3)^2\right)$$

In order to compute the three composite rotation angles θ_3, θ_2, and θ_1 we must solve for them from the analytic form of R given above.

If R is of the form:

$$R = \begin{bmatrix} a_{11} & a_{12} & a_{13} \\ a_{21} & a_{22} & a_{23} \\ a_{31} & a_{32} & a_{33} \end{bmatrix}$$

Then:

$$\theta_1 = \tan^{-1}\left(\frac{-a_{32}a_{12}}{\sqrt{-a_{12}(a_{33}a_{21} + a_{32}a_{31}a_{11})}}, \frac{-a_{33}a_{12}}{\sqrt{-a_{12}(a_{33}a_{21} + a_{32}a_{31}a_{11})}} \right)$$

$$\theta_2 = \tan^{-1}\left(-a_{31}, -\frac{\sqrt{-a_{12}(a_{33}a_{21} + a_{32}a_{31}a_{11})}}{a_{12}} \right)$$

$$\theta_3 = \tan^{-1}\left(\frac{-a_{21}a_{12}}{\sqrt{-a_{12}(a_{33}a_{21} + a_{32}a_{31}a_{11})}}, \frac{-a_{11}a_{12}}{\sqrt{-a_{12}(a_{33}a_{21} + a_{32}a_{31}a_{11})}} \right)$$

This solution fails if any two of θ_3, θ_2, and θ_1 are equal to zero, then the simple solutions are:

$$\text{if } a_{11} \cong 0$$

$$\theta_1 = \tan^{-1}(a_{32}, a_{22})$$

$$\theta_2 = \theta_3 = 0$$

$$\text{else if } a_{22} \cong 0$$

$$\theta_2 = \tan^{-1}(a_{13}, a_{33})$$

$$\theta_1 = \theta_3 = 0$$

$$\text{else if } a_{33} \cong 0$$

$$\theta_3 = \tan^{-1}(a_{21}, a_{11})$$

$$\theta_1 = \theta_2 = 0$$

$$\text{end}$$

3.4.3.3   Homogeneous Coordinates

A 3×3 rotation matrix is sufficient to describe the orientation of a coordinate frame, however it is incapable of describing the location of a coordinate frame without some sort of extension. If coordinate frame L_1 is located $\vec{p}_1$ away from L_0 with a rotation matrix of R_1^0 then any point $\vec{x}_0$ in L_0 can be transformed to L_1 by:

$$\vec{x}_1 = \vec{p}_1 + R_1^0 \vec{x}_0$$

Instead of handling this in two discrete steps (rotation and translation) we can simplify the process by introducing homogeneous coordinates and homogeneous coordinate transformation matrices. Coordinates that exist in $\Re^3$ will now be represented by vectors in $\Re^4$:

Given a point $\vec{p} = [p_1, p_2, p_3]^T$ in $\Re^3$, the homogeneous vector describing $\vec{p}$ will be:

$$\vec{q} = [p_1, p_2, p_3, 1]^T$$

The 4×4 transformation matrix T is now defined:

$$T = \begin{bmatrix} R & p \\ 0 & 1 \end{bmatrix}$$

Where R is a rotation matrix and p is a translation vector in $\Re^3$.

Using the first example above, where the point $\bar{x}_0$ in coordinate frame L_0 is transformed to L_1. Then:

$$\bar{q}_0 = \left[\bar{x}_0^{\,T}, 1\right]^T$$

$$T_1^0 = \begin{bmatrix} R_1^0 & \bar{p}_1 \\ 0 & 1 \end{bmatrix}$$

$$\bar{q}_1 = T_1^0 \bar{q}_0, \text{ then:}$$

$$\bar{x}_1 = H\bar{q}_1, \text{ where } H_{3\times 4} = \left[I_{3\times 3}, [0,0,0]^T\right]$$

3.4.4 Local Regression Smoothing

Although the marker location data has been filtered using a Woltring filter so that the first discrete derivatives are sufficiently smooth, some further data smoothing is necessary prior to taking the second discrete derivative to calculate accelerations. A typical causal discrete filtering scheme will introduce some phase-shift into the data set, and initial attempts with conventional low-pass acausal linear filters did not yield good results. Instead a locally weighted linear regression or LOESS smoothing function was used (Cleveland 1979).

Given a data set (x, y), where y is the dependent variable and x is an equally spaced independent variable. The locally-based "tricube" weighting function for the ith data point with smoothing span n is:

$$w_i(k) = \left(1 - \left|\frac{x_k - x_i}{0.5(n-1)}\right|^3\right)^3$$

Where:

$$k = i - \frac{n-1}{2} : i + \frac{n-1}{2}$$

With $n = 21$, the weighting function for the 11th data point is shown below:

Local Weights for the 11th data point and n = 21
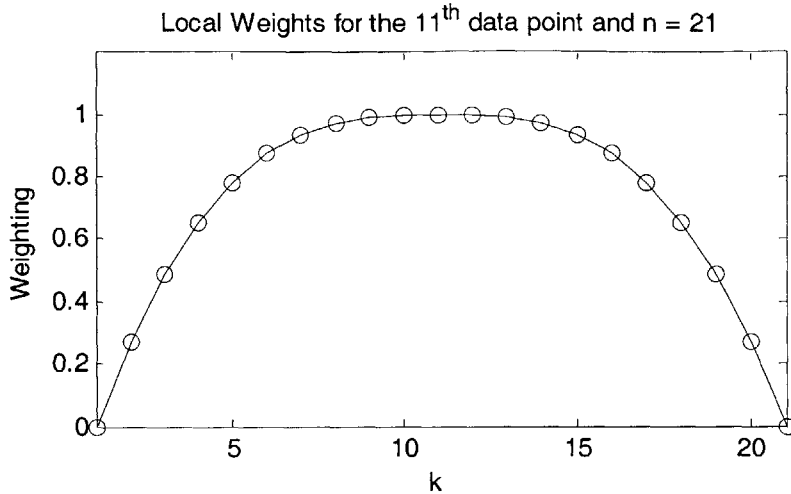
Figure 3.4.2 Example local regression weighting function for $n = 21$, and $i = 11$.

A new weighting vector, w, is calculated that has a shape similar to the one in figure 3.4.2 and is zero anywhere outside the smoothing span for every data point. A least-squares weighted linear regression is performed and used to calculate the smoothed value at the center of the span. Since the locally weighted linear regression is repeated for every data point the LOESS smoothing function is computationally intensive.

Instead of performing the locally weighted linear regression for every data point, an equivalent acausal finite impulse response (FIR) filter was found. The equivalent FIR filter is found by examination at the discrete impulse response of the LOESS smoothing function. A smoothing span of $n = 7$ was used to filter velocities before the second discrete derivative was taken. As interpreted from the chart below, the -3 dB corner frequency of the equivalent FIR filter is 13.51 Hz.
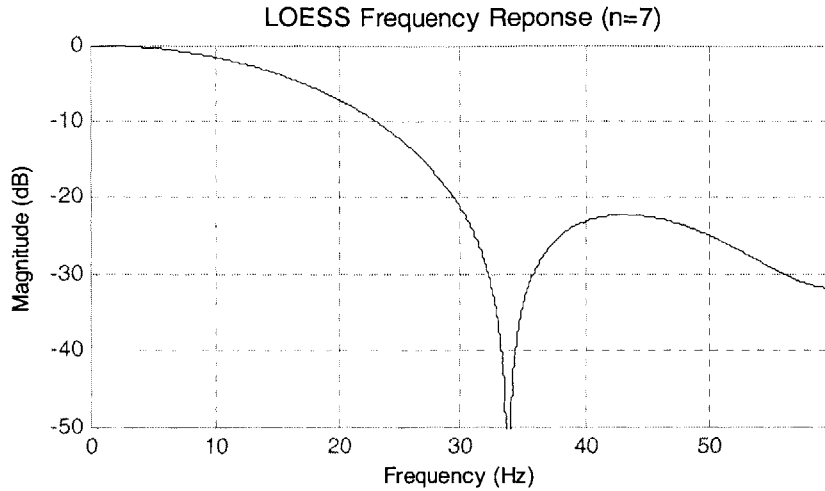
Figure 3.4.3 Frequency response of LOESS equivalent FIR filter. The (-3 dB) corner frequency is 13.51 Hz.

3.4.5   Discrete Derivatives of Time

Gait data is sampled at a rate of 120 Hz, for many analyses in this thesis it was necessary to differentiate this data with respect to time. The time derivative can be approximated with the first difference equation.

Given a dataset $\bar{x} = [x_1, x_2, \ldots, x_{N-1}, x_N]$ with sampling interval Δt.
Then the first difference equation approximation of the time derivative is:

$$\dot{x}_k = \frac{1}{\Delta t}(x_k - x_{k-1})$$

Taking the z-transform of the derivative approximation yields the following transfer function between the derivative estimate and the original dataset:

$$\frac{\dot{X}[z]}{X[z]} = D[z] = \frac{1}{\Delta t}\left(\frac{z-1}{z}\right)$$

This derivative estimate is quite sensitive to high frequency noise; the frequency response plot of the first difference equation with a sampling rate of 120 Hz is shown below.
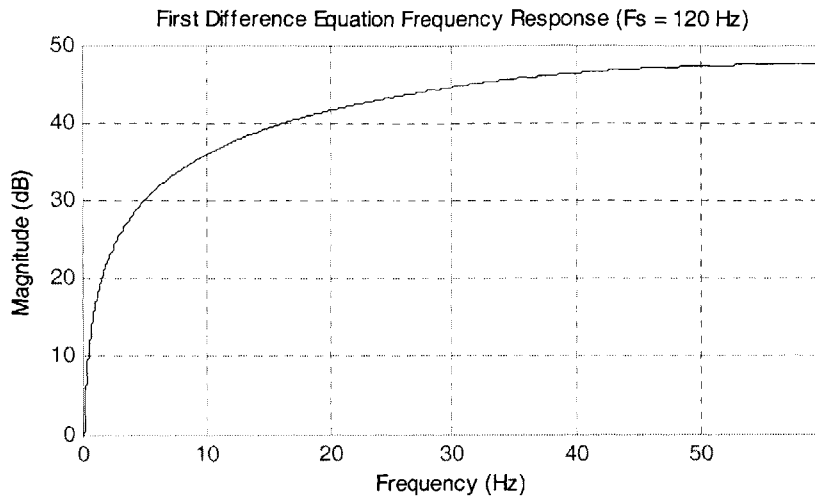
Figure 3.4.4 Frequency response of the first difference equation estimate of the time derivative.

Given the high-frequency sensitivity of the first difference equation derivative estimate, it is common to complement this filter with a suitable low-pass filter.

Where $\dot{x}_k$ is the causal first difference equation derivative estimate as given above, the filtered acausal derivative estimate is given by:

$$\dot{x}'_k = -\frac{1}{12}\dot{x}_{k-1} + \frac{7}{12}\dot{x}_k + \frac{7}{12}\dot{x}_{k+1} - \frac{1}{12}\dot{x}_{k+2}$$

The z-transform of the new derivative estimate equation is:

$$\frac{\dot{X}'[z]}{\dot{X}[z]} = z^2 F[z] = z^2 \frac{-z^3 + 7z^2 + 7z - 1}{12z^3}$$

The new frequency response of the low-pass filtered derivative estimate is:
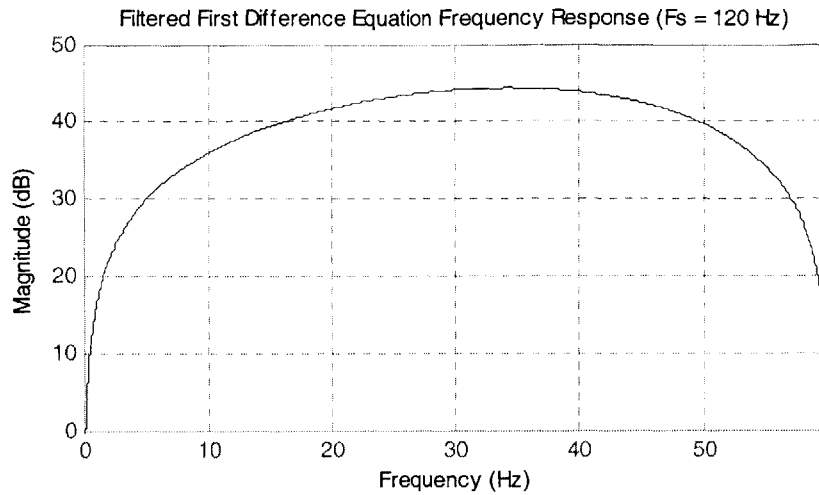
Figure 3.4.5 Frequency response of the filtered first difference equation estimate of the time derivative.

The total transfer function from the dataset to the filtered derivative estimate is shown below:

$$\frac{\dot{X}'[z]}{X[z]} = z^2 F[z]D[z] = \frac{z^2}{12\Delta t}\left(\frac{-z^4 + 8z^3 - 8z + 1}{z^4}\right)$$

The difference equation for the above transfer function is:

$$\dot{x}'_k = \frac{1}{12\Delta t}\left(-x_{k+2} + 8x_{k+1} - 8x_{k-1} + x_{k-2}\right)$$

Since the above difference equation is acausal, it cannot be used at the beginning or end of the data record to be differentiated with respect to time. In those cases for $\vec{x} = [x_1, x_2, \ldots, x_{N-1}, x_N]$, the following difference equations were used:

$$k = 1$$

$$\dot{x}_1' = \frac{1}{\Delta t}\left(-\frac{3}{2}x_1 + 2x_2 - \frac{1}{2}x_3\right)$$

$$k = 2$$

$$\dot{x}_2' = \frac{1}{\Delta t}\left(-\frac{1}{2}x_1 - \frac{1}{12}x_2 + \frac{2}{3}x_3 - \frac{1}{12}x_4\right)$$

$$k = N - 1$$

$$\dot{x}_{N-1}' = \frac{1}{\Delta t}\left(\frac{1}{12}x_{N-3} - \frac{2}{3}x_{N-2} + \frac{1}{12}x_{N-1} + \frac{1}{2}x_N\right)$$

$$k = N$$

$$\dot{x}_N' = \frac{1}{\Delta t}\left(\frac{1}{2}x_{N-2} - 2x_{N-1} + \frac{3}{2}x_N\right)$$

3.5 Determining Gait Events

During subject testing, a range of one to three total gait cycles of data was acquired. In order to analyze each gait cycle independently, it is necessary to partition the total dataset in to sub-datasets for each gait cycle. The gait cycle is defined by consecutive heel-strike events of the right foot. The problem arises however, that only one true heel-strike event is recorded by the right force plate. Additional ground contacts of the right foot, as well as toe off events must be estimated from kinematics.

3.5.1 Heel-Strike and Toe-Off from Force Plate Data

Determining heel-strike and toe-off gait events from force plate data is relatively simple. The vertical component of the normalized ground reaction force is analyzed, and a heel-strike or toe-off event is triggered if the magnitude crosses a critical value.

Given the ground reaction force from a force plate $F_r = [F_x, F_y, F_z]$, the normalized ground reaction force vector is:

$$\hat{F}_r = \frac{1}{M_{tot} \cdot g}[F_x, F_y, F_z]$$

An arbitrary crossover value of 0.05 normalized units was selected to determine the heel-strike and toe-off events. A sample normalized vertical ground reaction force plot, and the subsequent foot-contact events are shown below in figure 3.5.1.
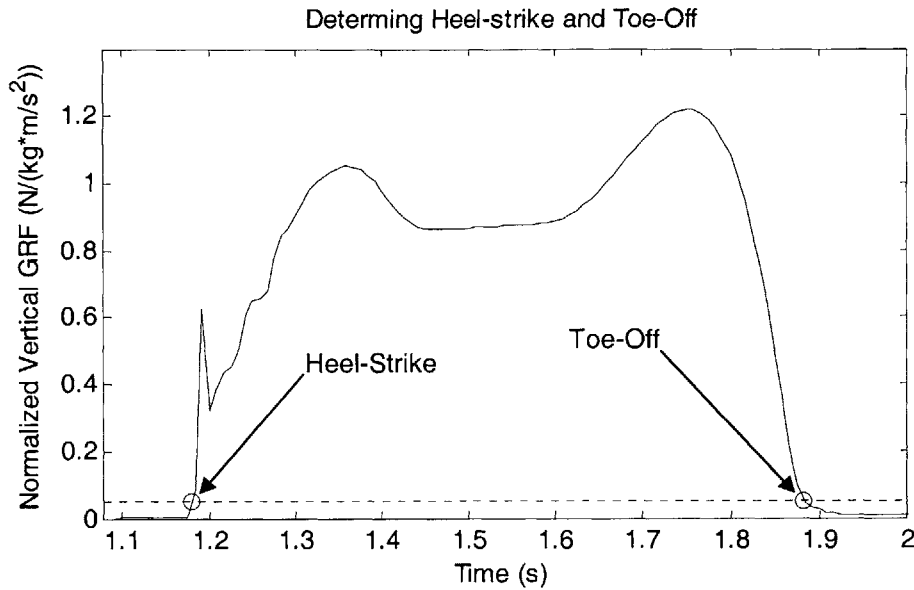
Figure 3.5.1 Determining heel-strike and toe-off events from normalized vertical ground reaction force data.

3.5.2   Estimation of Gait Events

The heel-strike and toe-off events were reasonably simple to determine when working within the gait cycle in which contact was made with the force plates. As there were only two force plates in use, for the right and left foot respectively, additional foot-contact events must be estimated from kinematics. Heel-strike and toe-off can be reasonably determined by analysis of the vertical position of the heel and toe markers respectively.

There is some degree of misalignment of the camera system so that any subject appears to be walking downhill slightly as they walk along the walkway in the motion laboratory. If a vertical marker position is to be used to estimate gait events, then this must first be adjusted.

1. With toe marker position $\bar{p}_{toe} = \lfloor p_x, p_y, p_z \rfloor$ find a general estimate of foot contact by examination of $\dot{p}_y$ and $\dot{p}_z$. If $|\dot{p}_y| \leq 0.05$ m/s and $|\dot{p}_z| \leq 0.02$ m/s then assume that the toe is on the ground.

2. Using only data from the roughly determined foot contact phase fit a linear curve to p_z versus p_y: $\hat{p}_z = m \cdot p_y + b$

3. Let p_z' be the adjusted vertical position so that $p_z' = p_z - m \cdot p_y$

4. If $t_{toe\,off}$ is the previous calculated time at toe off from force plate data, then the predicted time at the next toe off is calculated from the negative to positive zero crossing of $p_z' - p_z'(t_{toe\,off})$.

Sagittal View of Adjusted Toe Marker

Autocorrelated toe-off from kinematics

Toe-off predicted from force plate data

Horizontal Position (m)

Adjusted Vertical Position (m)
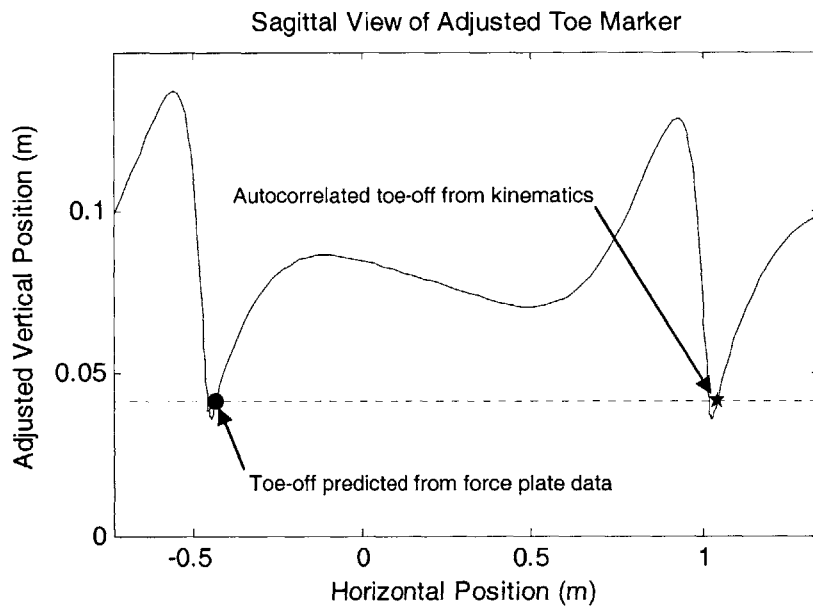
Figure 3.5.2 Estimation of toe-off from kinematical data for the toe marker.

Although the velocity of marker position data was used to determine roughly when the toe or heel was on the ground for adjusting position data, the position data were used for estimating gait events because of higher accuracy. The process for heel-strike would be the same as outlined above, only the heel marker would be used instead.

3.6   Body Modeling

The human body is a complex system consisting of a semi-rigid structure of 206 bones, cartilage, and tendon, covered with muscle and other soft tissue. In order to use motion capture data to derive meaningful quantitative information about subject gait a simplified mulit-segment model of the body must be used.

As early as 1680 Giovanni Alfonso Borelli estimated the location of the body center of mass by placing cadavers on a rigid platform and balancing them on a knife edge. Most efforts in body segment parameter estimation have involved work with cadavers to estimate the mass and mass center location of partitioned body segments (Dempster 1955, Chandler et al. 1975). Whitsett (1962) and Hanavan (1964) used a geometric model of the body consisting of spheres, ellipsoids, cylinders, truncated cones, and rectangular parallelepipeds along with body density information to predict segment mass, center of mass location, and moment of inertia for as many as 15 different segments. Zatsiorsky (1990) used a gamma ray scanning method to estimate body segment parameters for 16 body segments. The Zatsiorksy body segment parameter estimates were calculated from a large sample size of young college-aged subjects and were used to define the segment parameters in this thesis.

3.6.1   Segment Coordinate Frames

The body segment coordinate frames for the feet, shanks, thighs, hands, forearms, and upper arms were located and oriented directly from the modeled bones from Vicon BodyBuilder. The orientation and location of the pelvis, abdomen, chest, and neck-head were calculated using direct marker data since the 16 segment model used is slightly different from the Vicon software model.

Table 3.6.1 Body Segment Coordinate Frame Location and Orientation

Segment Number	Segment Name	Origin	x-axis
1	R. Foot	Right Calcaneus	Anteriorly toward the acropodion
2	L. Foot	Left Calcaneus	-
3	R. Shank	Right Knee Joint Center	Distally toward the ankle joint center
4	L. Shank	Left Knee Joint Center	-
5	R. Thigh	Right Hip Joint Center	Distally toward the knee joint center
6	L. Thigh	Left Hip Joint Center	-
7	R. Hand	Right Wrist Joint Center	Distally toward the 3rd dactylion
8	L. Hand	Left Wrist Joint Center	-
9	R. Forearm	Right Elbow Joint Center	Distally toward the wrist joint center
10	L. Forearm	Left Elbow Joint Center	-
11	R. Upper Arm	Right Shoulder Joint Center	Distally toward the elbow joint center
12	L. Upper Arm	Left Shoulder Joint Center	-
13	Pelvis	Omphalion Projection to Body Center	Inferiorly toward the center of the hips
14	Abdomen	Xyphoid Process Projection to Body Center	Inferiorly toward the omphalion
15	Chest	Cervicale Projection to Body Center	Inferiorly toward the xyphoid process
16	Head	Center of Head Markers	Inferiorly toward the cervicale
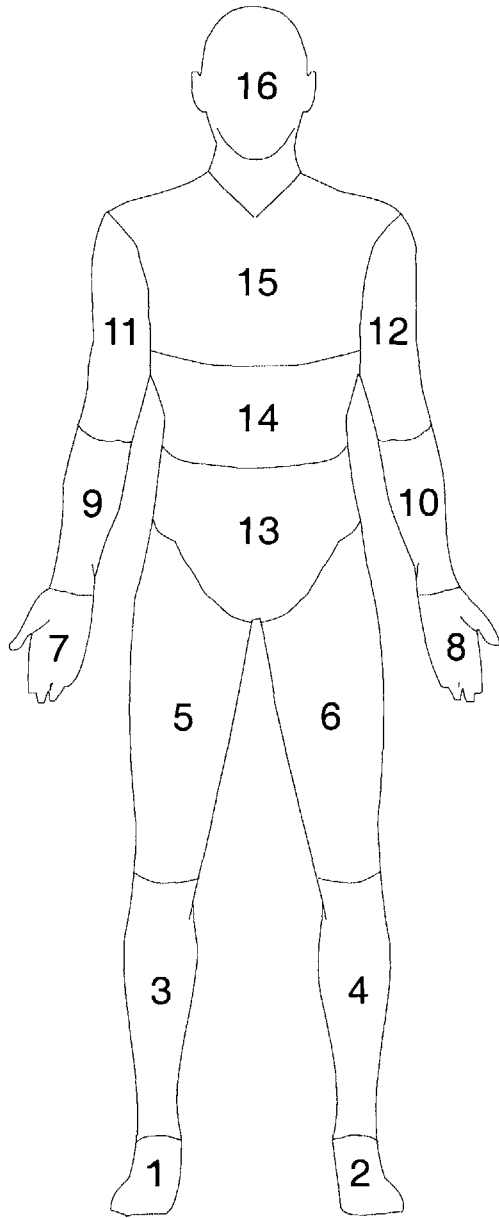
Figure 3.6.1 Sixteen segment body model based on the Zatsiorsky body segment parameter estimates.
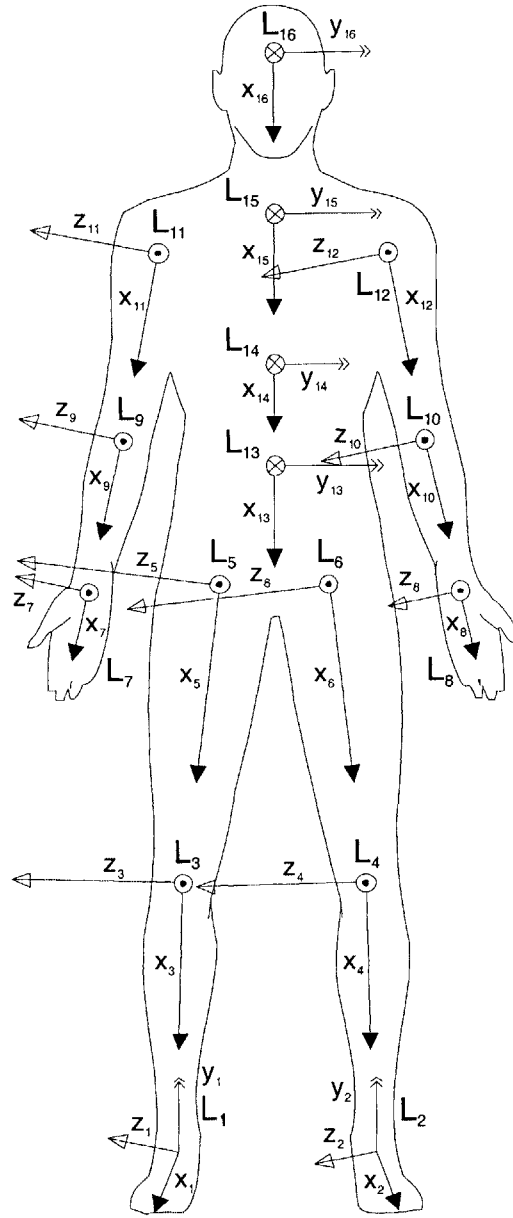
Figure 3.6.2 Local coordinate frames origins designated L_k. Axes oriented as shown.

3.6.2 Body Segment Parameter Estimation

Once coordinate frames have been defined we are able to model each of the sixteen segments of the body using predictions of: segment mass, longitudinal center of mass location, and radius of gyration. Zatsiorsky et al. (1990) published body segment

parameter data based upon subject anthropometric measurements. De Leva (1996) published adjustments to Zatsiorsky's data in which the radius of gyration and longitudinal center of mass location was based upon segment length. The de Leva adjustments allowed much more natural segment coordinate frame placement since typical segment lengths were defined between joint centers and not anthropometric landmarks.

Segment BSPs are calculated as follows for segment k :

$$m_k = \alpha_k \cdot M_{total}$$

$$I_k = m_k \cdot l_k^{\,2} \cdot \begin{bmatrix} \beta_{k\,long}^{\;2} & 0 & 0 \\ 0 & \beta_{k\,sag}^{\;2} & 0 \\ 0 & 0 & \beta_{k\,tran}^{\;2} \end{bmatrix}$$

Where α_k is the percentage mass coefficient for the kth segment, $\beta_{k\,long}$, $\beta_{k\,sag}$, and $\beta_{k\,tran}$ are the sagittal, transverse, and longitudinal radii of gyration constants respectively, taken from table 3.6.2.

Table 3.6.2 de Leva adjustments to Zatsiorksy body segment parameter estimates.

Segment	Endpoints		Mass (%)		Longitudinal CM Position (%)		Sagittal r (%)		Transverse r (%)		Longitudinal r (%)	
	Origin	Termination	F	M	F	M	F	M	F	M	F	M
Head	VERT	CERV	6.68	6.94	48.41	50.02	27.10	30.30	29.50	31.50	26.10	26.10
Upper Trunk	CERV	XYPH	15.45	15.96	50.50	50.66	46.60	50.50	31.40	32.00	44.90	46.50
Mid Trunk	XYPH	OMPH	14.65	16.33	45.12	45.02	43.30	48.20	35.40	38.30	41.50	46.80
Lower Trunk	OMPH	HJCC	12.47	11.17	49.20	61.15	43.30	61.50	40.20	55.10	44.40	58.70
Upper Arm	SJC[a]	EJC	2.55	2.71	57.54	57.72	27.80	28.50	26.00	26.90	14.80	15.80
Forearm	EJC[b]	WJC	1.38	1.62	45.59	45.74	26.10	27.60	25.70	26.50	9.40	12.10
Hand	WJC[c]	DAC3[d]	0.56	0.61	34.27	36.24	24.40	28.80	20.80	23.50	15.40	18.40
Thigh	HJC[e]	KJC	14.78	14.16	36.12	40.95	36.90	32.90	36.40	32.90	16.20	14.90
Shank	KJC[f]	AJC[g]	4.81	4.33	43.52	43.95	26.70	25.10	26.30	24.60	9.20	10.20
Foot	HEEL[h]	TTIP[i]	1.29	1.37	40.14	44.15	29.90	25.70	27.90	24.50	13.90	12.40

a Shoulder joint center, b Elbow joint center, c Wrist joint center, d 3rd Dactylion, e Hip joint center, f Knee joint center, g Ankle joint center, h Calcaneus of the heel, i Acropodion.

Segment masses are defined as a percentage of total body mass. Segment longitudinal center of mass locations and radii of gyration are defined as a percentage of the segment length from origin to termination.

Once coordinate frames have been defined we are able model each of the sixteen segments of the body using predictions of: segment mass, longitudinal center of mass location, and radius of gyration.

3.6.3   Locating Body Segment Centers of Mass

The segmental coordinate frames are typically located at a proximal joint, e.g. the shank coordinate frame is located at the knee joint center oriented with the x-axis distally toward the ankle joint center and the z-axis normal to the sagittal plane. It is necessary to transform the segment mass center in the segmental coordinate frame to the global coordinate frame during gait analysis.

The center of mass for segment k can be located in the global frame:

Given T_0^k, the homogeneous transformation matrix from the kth coordinate frame to the lab frame, then:

$$\vec{x}_{k\,cm} = H \cdot T_0^k \cdot [v_k \cdot l_k, 0, 0, 1]^T$$

Where v_k is the longitudinal center of mass position scalar from table 3.6.2.

3.6.4   Body Center of Mass

A point of particular interest when studying gait is the motion of the body center of mass (BCM). The BCM is the mass weighted average of the 16 body segments divided by the total body mass.

Given m_k, the mass of the kth segment and $\vec{x}_k$, the position of the kth segment mass center in the global frame, then:

$$M_{tot} = \sum_{k=1}^{16} m_k$$

$$\vec{x}_{BCM} = \frac{1}{M_{tot}} \sum_{k=1}^{16} m_k \cdot \vec{x}_k$$

3.6.5   Body Linear Momentum

The linear momentum of the body is the derivative of the BCM multiplied by the total system mass, or it can be calculated in series form taking the derivatives of the individual segment mass locations.

Let $\bar{p}_k$ be the linear momentum of the kth segment.

$$\bar{p}_k = m_k \frac{d}{dt}(\bar{x}_k) = m_k \cdot \dot{\bar{x}}_k$$

Then:

$$\bar{p}_{tot} = \sum_{k=1}^{16} m_k \cdot \dot{\bar{x}}_k = M_{tot} \cdot \dot{\bar{x}}_{BCM}$$

3.6.6   Body Angular Momentum

Calculating the total body angular momentum is not nearly as simple as the linear momentum. The inertia tensors for each segment must be transformed to the global coordinate frame and multiplied by the angular velocity of the respective coordinate frames, then summed with the angular momentum of each segment mass center about the BCM.

Let $\bar{L}_k$ be the angular momentum of the kth segment about the BCM, and given R_0^k, the 3×3 rotation matrix from the kth coordinate frame to the lab frame.

$$\bar{L}_k = \bar{L}_{k\,remote} + \bar{L}_{k\,local}$$
$$\bar{L}_{k\,remote} = m_k \cdot (\bar{x}_k - \bar{x}_{BCM}) \times (\dot{\bar{x}}_k - \dot{\bar{x}}_{BCM})$$
$$\bar{L}_{k\,local} = R_0^k \cdot I_k \cdot R_k^0 \cdot \bar{\omega}_k$$

Where $\bar{\omega}_k$ is the angular velocity of the kth coordinate frame and I_k is the inertia tensor of the kth segment with respect to its coordinate frame.

Finding the local component of the angular momentum involves the rotation matrix, inertia tensor, and the angular velocity of the segmental coordinate frame. Determining the angular velocity of the segmental coordinate frame involves some additional steps.

3.6.6.1   First Method

Using the inverse fundamental yaw-pitch-roll formulation as described in section 3.4.3.2, three angles describing the orientation of the coordinate frame θ_1, θ_2, and θ_3 are found.

Where:

$$YPR(\theta_3,\theta_2,\theta_1) = R_z(\theta_3)R_y(\theta_2)R_x(\theta_1)$$

Then the $\vec{\omega}_k$ can be calculated:

$$\vec{\omega}_k = \begin{bmatrix} 0 \\ 0 \\ \dot{\theta}_3 \end{bmatrix} + R_z(\theta_3)\cdot\begin{bmatrix} 0 \\ \dot{\theta}_2 \\ 0 \end{bmatrix} + R_z(\theta_3)R_y(\theta_2)\cdot\begin{bmatrix} \dot{\theta}_1 \\ 0 \\ 0 \end{bmatrix}$$

3.6.6.2   Second Method

Alternatively the angular velocity can be found be differentiating the 3×3 rotation matrix R_0^k with respect to time and multiplying by R_k^0. The added advantage of this is that the elements of the rotation matrix R_0^k should change in a continuous manner and will not suffer from any wraparound issues as $\theta_{1,2,3}$ goes from $0\ldots2\pi$ or from any issues surrounding gimbal lock. The second method of calculating angular velocities was used in all analyses for this thesis.

$$W = \frac{d}{dt}\left(R_0^k\right)\cdot R_k^0$$

Where W is a skew-symmetric singular matrix:

$$W = \begin{bmatrix} 0 & -\omega_z & \omega_y \\ \omega_z & 0 & -\omega_x \\ -\omega_y & \omega_x & 0 \end{bmatrix}$$

Comparison of Methods for Calculating ω
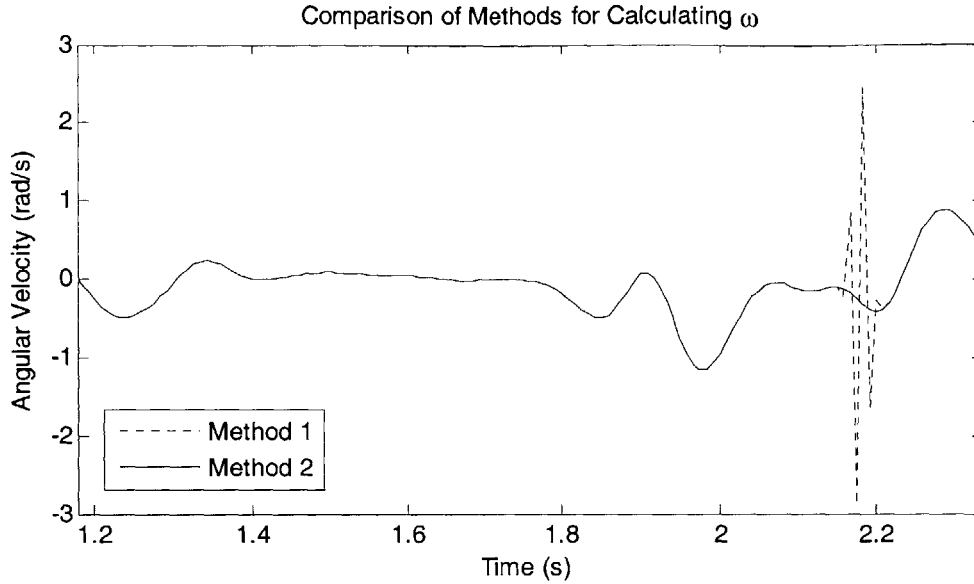
Figure 3.6.3 Comparison of two methods to calculate the angular velocity of the segmental coordinate frame with respect to the global coordinate frame. The first method has problems when the derivatives of the rotation angles are used. Using the second method ensures smooth velocity plots and no extra data processing is necessary to remove data artifacts.

3.6.7 Gait Energetics

The total energy in any system of objects is naturally partitioned into gravitational potential energy, translational kinetic energy, and rotational kinetic energy.

$$E_{potential} = \sum_{k=1}^{16} m_k g \bar{x}(3)_k$$

$$E_{kin-translational} = \sum_{k=1}^{16} \frac{1}{2} m_k \dot{x}_k{}^T \dot{x}$$

$$E_{kin-rotational} = \sum_{k=1}^{16} \frac{1}{2} \bar{\omega}_k{}^T R_0^k I_k R_k^0 \bar{\omega}_k$$

By the König theorem, the translational kinetic energy can be decomposed into the kinetic energy of the body center of mass and the kinetic energy of the body segments with respect to the BCM.

$$E_{kin-translational} = \sum_{k=1}^{16} \frac{1}{2} m_k \dot{x}_k{}^T \dot{x} = \frac{1}{2} M_{tot} \dot{x}_{BCM}{}^T \dot{x}_{BCM} + \sum_{k=1}^{16} \frac{1}{2} m_k \dot{x}_{k-BCM}{}^T \dot{x}_{k-BCM}$$

- 56 -

Total system energy is partitioned into two quantities: external energy associated with the movement of the BCM and internal energy associated with the movement of the segments about the BCM.

$$E_{External} = M_{tot}\, g\bar{x}(3)_{BCM} + \frac{1}{2}M_{tot}\,\dot{\bar{x}}_{BCM}^{\ T}\dot{\bar{x}}_{BCM}$$

$$E_{Internal} = \sum_{k=1}^{16}\frac{1}{2}m_k\,\dot{\bar{x}}_{k-BCM}^{\ T}\dot{\bar{x}}_{k-BCM} + \sum_{k=1}^{16}\frac{1}{2}\bar{\omega}_k^{\ T}R_0^k I_k R_k^0 \bar{\omega}_k$$

Gait analysis has revealed that partitioning of the external energy into that which is associated with the vertical axis (vertical kinetic and gravitational potential) and the energy associated with the horizontal axes (forward kinetic energy) results in two energy curves which are roughly equal in magnitude and out of phase (Saibene 1990).

$$E_{Vert-External} = M_{tot}\, g\bar{x}(3)_{BCM} + \frac{1}{2}M_{tot}\,\dot{x}(3)_{BCM}^{\ 2}$$

$$E_{Horiz-External} = \frac{1}{2}M_{tot}\,\dot{x}(1)_{BCM}^{\ 2} + \frac{1}{2}M_{tot}\,\dot{x}(2)_{BCM}^{\ 2}$$

When this analysis is expanded to include the internal energy as well, the results are not nearly the same; the internal energy tends to be in phase with the gravitational potential, so the two energy curves do not cancel nearly as well.

$$E_{Vert-Total} = M_{tot}\, g\bar{x}(3)_{BCM} + \sum_{k=1}^{16}\frac{1}{2}m_k\,\dot{x}(3)_k$$

$$E_{Horiz-Total} = \sum_{k=1}^{16}\frac{1}{2}m_k\left(\dot{x}(1)_k^{\ 2} + \dot{x}(2)_k^{\ 2}\right) + \sum_{k=1}^{16}\frac{1}{2}\bar{\omega}_k^{\ T}R_0^k I_k R_k^0 \bar{\omega}_k$$

3.6.8   Joint Torque Calculations

The joint torques were calculated for the right ankle, knee, and hip joint using a recursive Newton-Euler algorithm. The recursive Newton-Euler algorithm works well for articulated systems like the leg. The forward pass of the algorithm progresses from the base to the last link calculating link accelerations and velocities. The reverse pass proceeds in the opposite manner from the last link towards the base calculating reaction torques and forces. Since the joint accelerations and velocities are already known from previous steps, the forward pass of the Newton-Euler algorithm can be bypassed

altogether and only the reverse pass is used. The foot is assumed to be the last link of the articulated chain, and the ground reaction force data are used to calculate the load and torque applied to the last link.

Let:

$\vec{\omega}_1$, $\vec{\omega}_2$, and $\vec{\omega}_3$ be the angular velocity of the right foot, shank, and thigh.

$\vec{x}_1$, $\vec{x}_2$, and $\vec{x}_3$ be the global frame mass center locations of the right foot, shank, and thigh.

$\vec{p}_1$, $\vec{p}_2$, $\vec{p}_3$, and $\vec{p}_4$ be the global frame locations of the right foot center of pressure, ankle joint center, knee joint center, and hip joint center.

$\vec{F}_0$ be the negative of the ground reaction force measured from the right force plate.

$\vec{\tau}_0$ be zero as there is no external torque applied to the foot if the ground reaction force is applied at the center of pressure.

Then:

$$\text{for } k = 1:3$$
$$\Delta \vec{r}_k = \vec{x}_k - \vec{p}_k$$
$$\Delta \vec{s}_k = \vec{p}_k - \vec{p}_{k+1}$$
$$\vec{F}_k = \vec{F}_{k-1} + m_k \cdot [0,0,g]^T + m_k \cdot \ddot{\vec{x}}_k$$
$$\vec{\tau}_k = \vec{\tau}_{k-1} - (\Delta \vec{r}_k + \Delta \vec{s}_k) \times \vec{F}_k + \Delta \vec{r}_k \times \vec{F}_{k-1} + R_0^k I_k R_k^0 \dot{\vec{\omega}}_k + \vec{\omega}_k \times (R_0^k I_k R_k^0 \vec{\omega}_k)$$
$$\text{end}$$

The $\vec{\tau}$ calculated are in the global coordinate frame, the torque must be transformed back into the segmental coordinate frame:

$$\vec{\tau}_k' = R_k^0 \cdot \vec{\tau}_k$$

3.7   Nonparametric Statistical Methods

Nonparametric statistics are based on data descriptors such as median, mode, and range, which differ from conventional parametric statistics of mean, standard deviation, etc. Nonparametric statistics are best used when analyzing data sets that

are small and where very little is known about the data distribution. Ten subjects were involved in testing, and at most only seven trials were conducted per weighting condition. If certain trials had to be rejected in post-processing the sample size was even lower. Since the sample size is small, the variances of the gait parameters are not well understood so that no conclusions can be made about their distribution. Additionally, nonparametric statistical comparisons are typically less powerful than their parametric counterparts; however is an aid in this research as it helps to isolate only the most salient differences between data sets.

3.7.1   Wilcoxon Matched Pairs Signed Rank Test

Wilcoxon (1945) presents a method that allows a repeated measures analysis of variance test. This test is very powerful as it can tell can tell us not only that a difference exists between two sample sets, but quantitatively the magnitude of the difference between the two as well.

Given two data sets $\vec{X}$ and $\vec{Y}$ where each pair of measurements (X_i, Y_i) is from the same subject. The null hypothesis is that the median difference between $\vec{X}$ and $\vec{Y}$ is zero. That is:

$$M_D = \text{median}(\vec{Y} - \vec{X})$$
$$H_0 : M_D = 0$$
$$H_1 : M_D \neq 0$$

The steps then to determine whether to reject the null hypothesis with α level significance are:

1. Obtain the signed differences
$$D_i = Y_i - X_i$$
2. Rank the absolute values of the signed differences
$$|D_i| = |Y_i - X_i|$$
$$\beta_i = \text{rank}(|D_i|)$$
3. Assign each of the ranks with the sign of the differences
$$\vartheta_i = \text{sgn}(D_i) \cdot \beta_i$$
4. The test statistics for one-sided tests are the sum of the ranks with the same sign

$$T_+ = \sum_{i=1}^{N} \chi_i \quad \text{where} \quad \chi_i = \begin{cases} \vartheta_i, & \vartheta_i > 0 \\ 0, & \text{otherwise} \end{cases}$$

$$T_- = \sum_{i=1}^{N} \chi_i \quad \text{where} \quad \chi_i = \begin{cases} |\vartheta_i|, & \vartheta_i < 0 \\ 0, & \text{otherwise} \end{cases}$$

5. For the two-tailed test, the test statistic is the minimum of T_+ and T_-.

$$T = \min(T_+, T_-)$$

6. For ties of $|D_i|$, the average of the ranks that would otherwise be assigned is given to them.

7. Reject H_0 with α level of significance if calculated test statistic T is smaller than or equal to $T_{critical}$ calculated from sample size n and tabulated data. (see appendix).

3.7.2 Signed Rank Test Median Confidence Intervals

It is of principle interest not only to predict that the median difference between two sets of observations is non-zero, but also to predict the magnitude of difference of medians and confidence intervals surrounding that estimated difference.

The steps to calculate the estimated median and corresponding confidence intervals are:

1. Obtain the signed differences
$$D_i = Y_i - X_i$$

2. Calculate every possible average of combinations of $\vec{D}$
for $i = 1 : n$

    for $j = i : n$

$$u_{(i-1)n+j-\frac{1}{2}(i^2-i)} = \frac{1}{2}(D_i + D_j)$$

    end

  end

There will be a total of $\frac{1}{2}(n^2 + n)$ total averages.

3. The median of $\vec{u}$ will be the estimate of the median difference of populations.

$$\hat{M}_{\bar{Y}-\bar{X}} = \text{median}(\vec{u})$$

4. For a two-tailed confidence interval for $(1-\alpha)$ confidence use tabulated data tables for sample size n and $P = 0.5 \cdot \alpha$ to determine $T_{critical}$.

5. The endpoints of the $(1-\alpha)$ confidence interval are the Kth largest and smallest values of $\vec{u}$.

$$K = 1 + T_{critical}$$
$$\vec{u}' = \text{sort}(\vec{u})$$
$$\hat{M}_{min} = \vec{u}'_K, \quad \hat{M}_{max} = \vec{u}'_{n-K+1}$$

3.8   Gait Parameter Definitions

This section contains a general review of how various gait parameters were defined. Section 3.8.1, 3.8.2, 3.8.3 define the peak kinematic and kinetic parameters for the ankle, knee, and hip respectively. Section 3.8.4 details the general stride parameters and their definitions. Section 3.8.5 contains additional definitions for body center of mass movement, root mean square signal strength, signal cancellation, and energy recovery.

3.8.1 Ankle Parameter Definitions
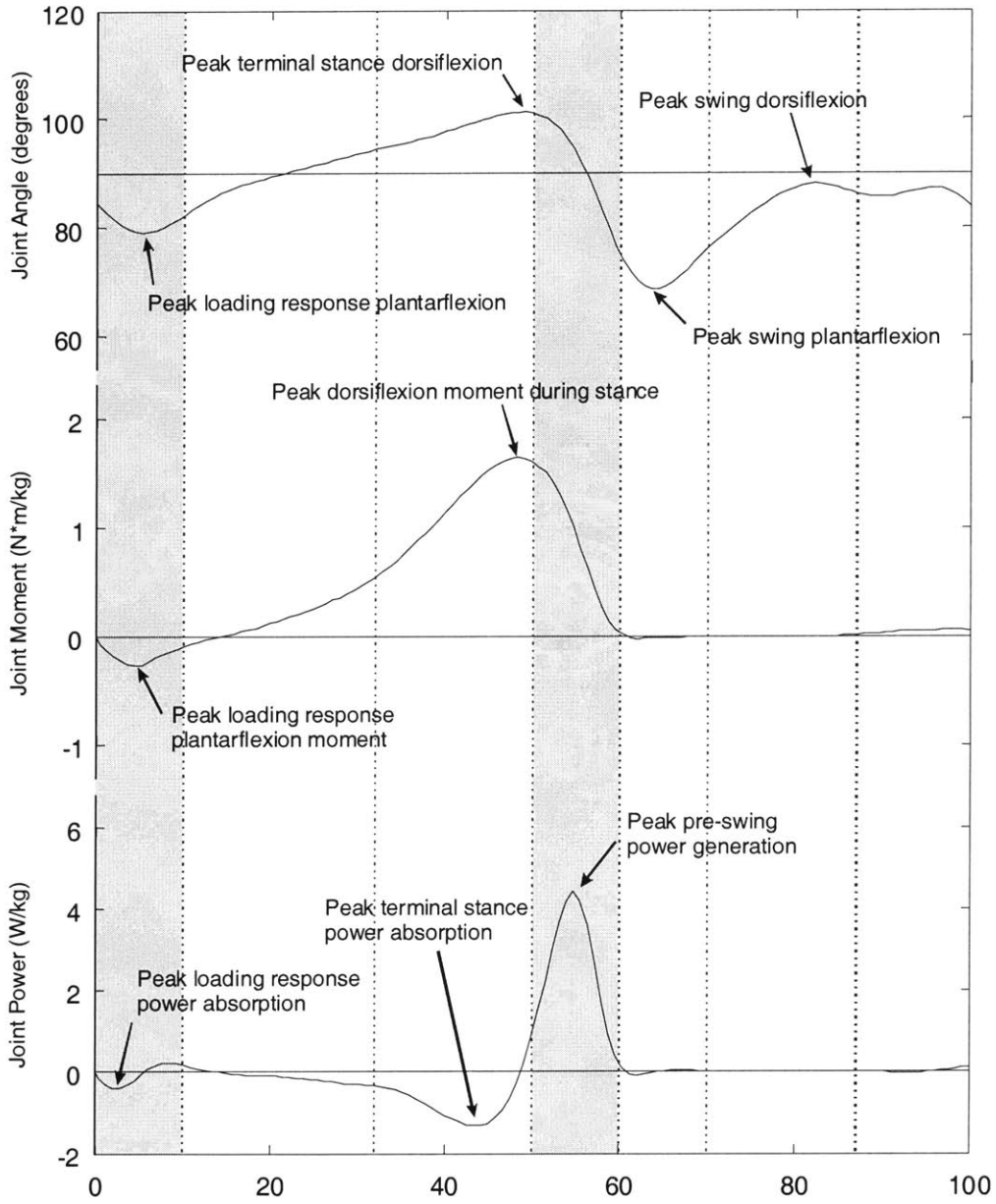
Figure 3.8.1 Ankle parameter definitions for angle, torque, and power.

3.8.2 Knee Parameter Definitions
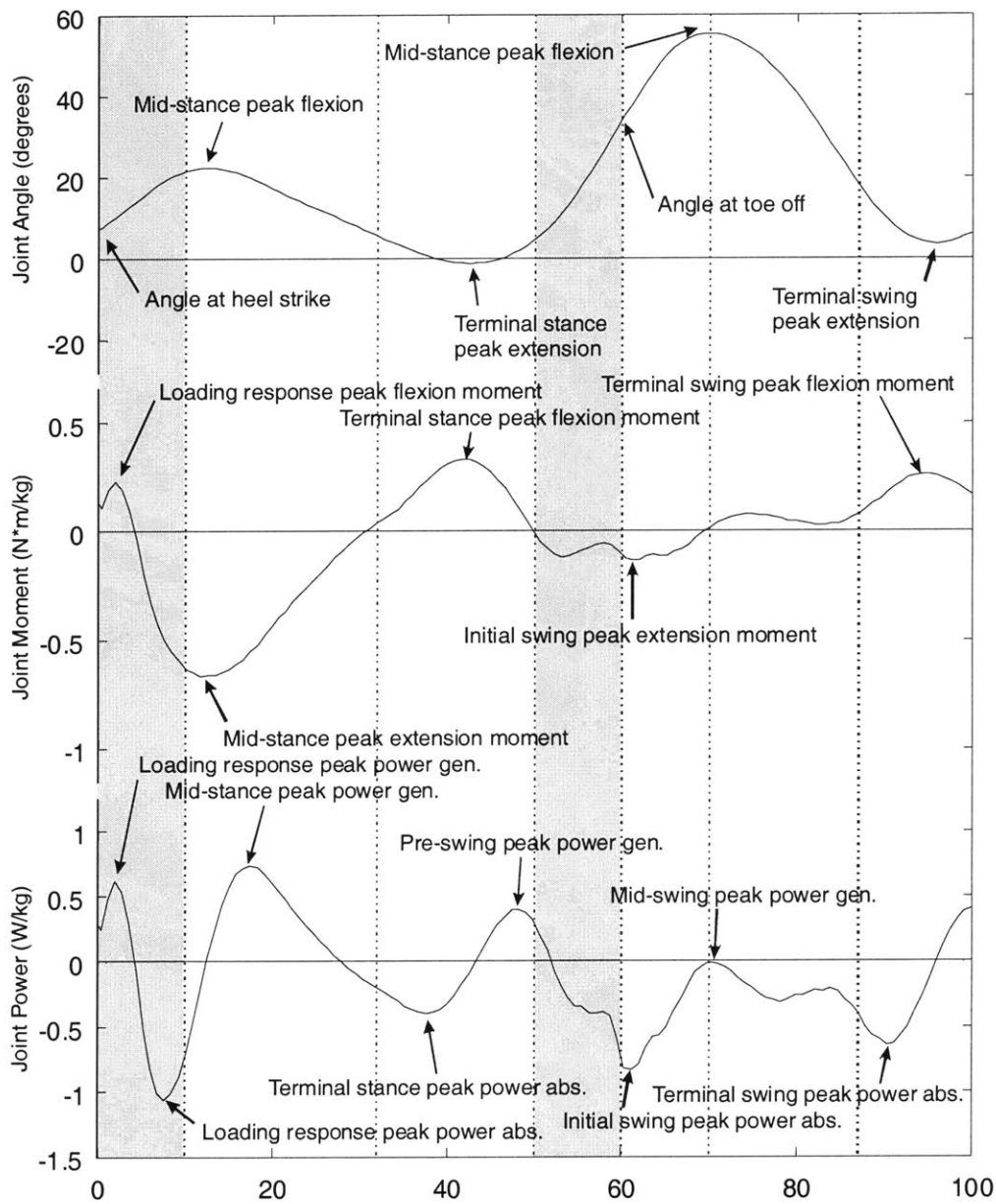
Figure 3.8.2 Knee parameter definitions for angle, torque, and power.

3.8.3   Hip Parameter Definitions
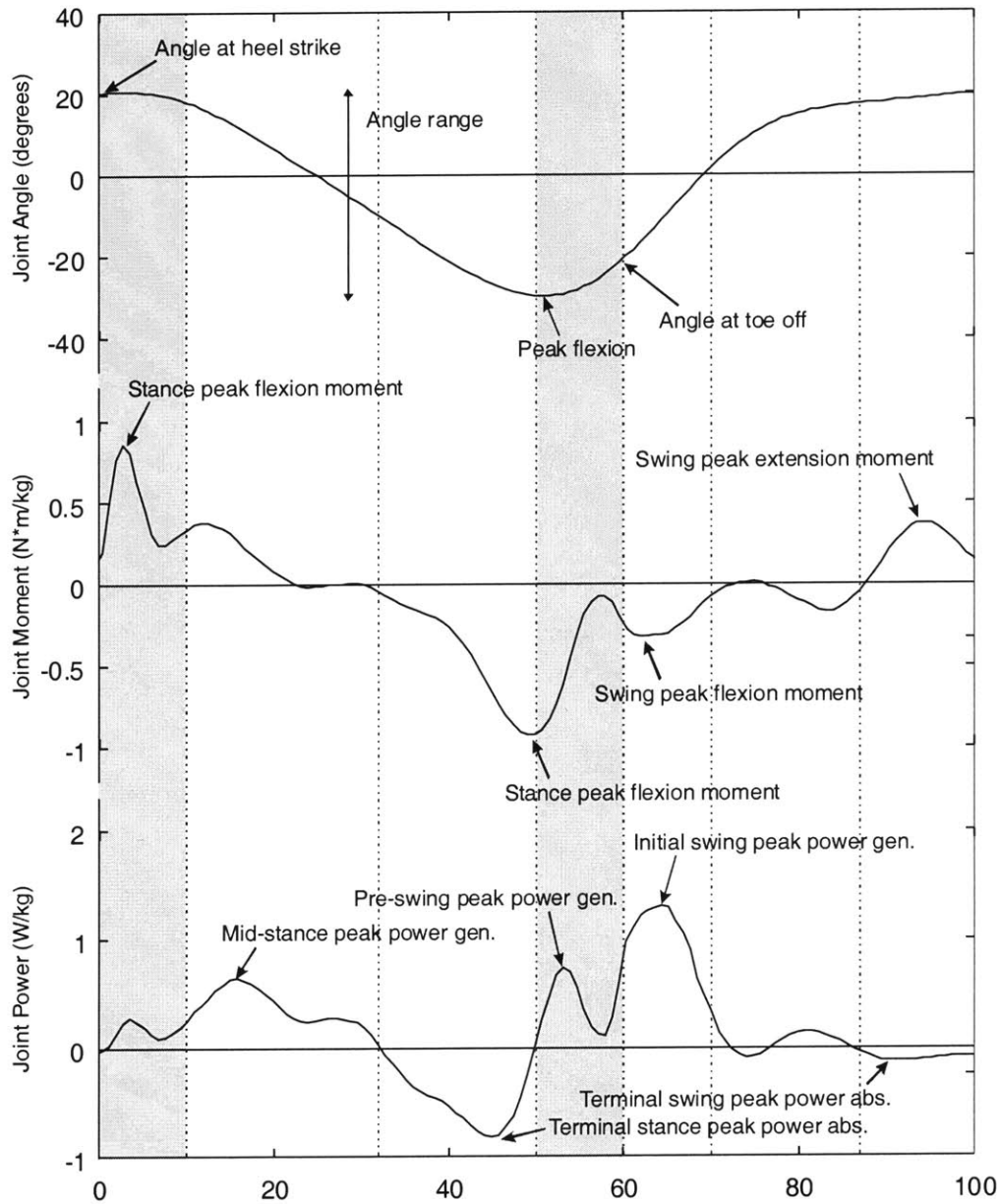
Figure 3.8.3 Hip parameter definitions for angle, torque, and power.

3.8.4   Stride Parameter Definitions

Step Length: The distance between the feet during double support from a
                      common reference point, e.g. the heel.

Stride Length:	The distance traveled by the foot during one gait cycle.
Step Time:	The time from toe off to heel strike, i.e. the duration of swing phase for one leg.
Stride Time:	The period of the gait cycle.
Walking Speed:	The average forward velocity of the body center of mass averaged over the gait cycle.

Figure 3.8.4 Methodology for determining stride length and step length.
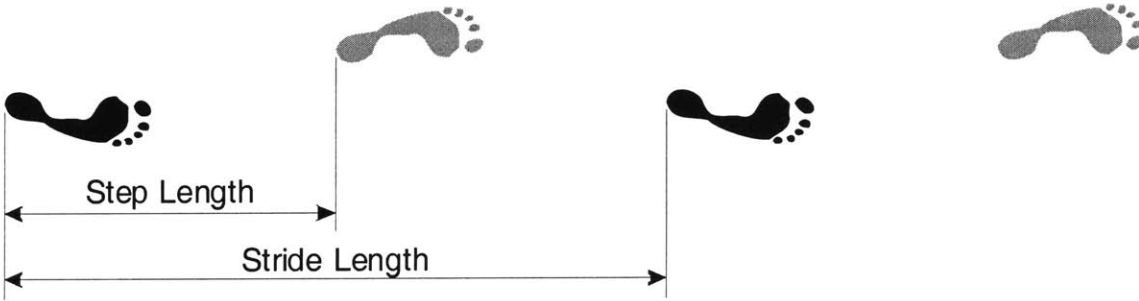
3.8.5   Additional Parameters

3.8.5.1   BCOM Distance from Linear Fit

There is some misalignment in the camera system used to acquire marker kinematic location data. To account for this misalignment and for the likelihood that subjects did not walk perfectly along the positive y-axis of the lab frame, body center of mass motion (BCOM) parameters were based upon the residuals from the linear regression of the body center of mass location.

Given the center of mass location $\bar{x}_{BCM}$ and time vector $\vec{t}$, where:

$$\bar{x}_{BCM} = \frac{1}{M_{tot}} \sum_{k=1}^{16} m_k \cdot \vec{x}_k$$

$$\vec{t} = [t_1, t_2, \ldots, t_N]$$

Let:

$$X_{BCM} = [\bar{x}(1)_{BCM}, \bar{x}(2)_{BCM}, \ldots, \bar{x}(N)_{BCM}]_{3 \times N}$$

$$T = [\vec{t}^T, \text{ones}(N,1)]_{N \times 2}$$

Then the distance of the body center of mass away from the linear fit is:

$$\overline{X}_{BCM} = X_{BCM} - \left(T \cdot \left(T^T \cdot T\right)^{-1} \cdot T^T \cdot X_{BCM}\right)^T$$

3.8.5.2   Root Mean Square Parameters

The root mean square of a signal is a general estimate of the magnitude of that signal. In the discrete case, it is equivalent to the standard deviation of a sample set if the mean is zero. The root mean square (RMS) of various torques, powers, and angular momentums was examined to determine if there was some information about the gait data that would not ordinarily be determined by just determining the maxima and minima.

Given a signal $\bar{x}$, where:

$$\bar{x} = [x_1, x_2, \ldots, x_N]$$

Then the root mean square of $\bar{x}$ is:

$$x_{RMS} = \left(\frac{1}{N} \sum_{i=1}^{N} x_i^2\right)^{\frac{1}{2}}$$

3.8.5.3   Percent Signal Cancellation Parameters

In analysis of the angular momentum of the body segments about the body center of mass, it was determined that a metric was needed to determine the degree to which the signals cancelled each other. From that need, an equation based upon individual and summed signal variances was postulated, that has been used quite often in this thesis with good results.

Given N signals in time:

$$\bar{x}_1, \bar{x}_2, \ldots, \bar{x}_N$$

Where:

$$\bar{x}_k = [x_{k1}, x_{k2}, \ldots, x_{kM}]$$

Then the percentage signal cancellation of the N signals is:

$$P = 100 \cdot \left(1 - \frac{\sigma^2_{1+2+...+N}}{\left(\sigma_1 + \sigma_2 + ... + \sigma_N \right)^2} \right)$$

Where σ_k, the standard deviation of the kth signal is:

$$\sigma_k = \left(\frac{1}{M} \sum_{i=1}^{M} \left(x_{ki} - \bar{x}_k \right)^2 \right)^{\frac{1}{2}}$$

3.8.5.4   Percentage Energy Recovery Parameters

Normal walking involves a cyclical energy transfer between gravitational potential and kinetic energy of the body center of mass (Willems et al. 1995). Energy recovery is a metric of how efficiently energy is converted from one form to the other; if the gravitational potential and kinetic energy are inverted versions of each other recovery will 100%. The definition shown below has been extended for any arbitrary number of energy partitions.

Given N energy signals in time:

$$\bar{E}_1, \bar{E}_2, ..., \bar{E}_N$$

Where:

$$\bar{E}_k = \left[E_{k,1}, E_{k,2}, ..., E_{k,M} \right]$$

Let:

$$W_k = \sum_{j=1}^{M-1} \left| E_{k,j+1} - E_{k,j} \right|$$

Then the percentage energy recovery for the N signals is:

$$R = 100 \cdot \left(1 - \frac{W_{1+2+...+M}}{W_1 + W_2 + ... + W_M} \right)$$

3.9   Virtual Mass Analysis

In experimental subject testing at the Motion Laboratory, subjects walked under two distinct load conditions: normal unloaded walking and walking with a 5 kg mass on the right leg. Thus, there were two kinematic datasets of interest. In the analysis of each kinematical data set a model of the body was used that should be a reasonable approximation of the true morphology. Using each kinematic set of data two abiologic analyses were performed: normal kinematics with a virtual mass placed on the right shin and loaded kinematics without the 5 kg mass. Comparisons of the loaded dataset versus the normal dataset are necessary to determine the presence of any invariant parameters due to added mass; however these comparisons were not very useful in elucidating the chief components of the biologic performance criterion because they represent two separate optimal loading conditions and an ideal comparison would be between an optimal and suboptimal solution.

The assumption has been made that each kinematic data set represents an optimal solution for their respective morphologies, i.e. loaded and unloaded. So that placing a virtual mass on the shank during analysis will represent a suboptimal solution for use in comparison to the true optimum. This method is a stronger approach than using any arbitrary kinematical dataset and concluding that it is suboptimal since the source of the data is a true biologic gait pattern, and it is assumed that unloaded symmetric walking is a "starting point" which will then be reorganized to optimize the performance criterion. While this mode of analysis can never be powerful enough to validate a suggested cost function; it can be used as a method to reject potential cost functions. If a kinematic solution is presented as the optimal solution to the biological optimization problem, then the solution is true if and only if all other solutions have a higher evaluation of the objective function. So that, if at least one solution has a lower cost the solution can be rejected. Since it is assumed that the dataset for loaded walking consists of a true solution, then the converse can be applied that if at least one known suboptimal solution results in a lower evaluation of the cost function, then the cost function can be rejected. Furthermore, the general assumption is made that the gradient is sufficiently steep from the known suboptimal solution to the optimum that individual parameters of the cost function can be evaluated in an effort to reveal the chief components of the biologic cost function.
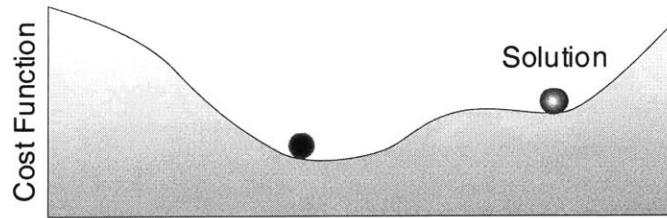
Figure 3.9.1 Virtual mass analysis logic. If at least one solution can be found that has a lower value of the cost function than the known solution, the solution can be rejected, or using the converse the cost function can be rejected. The weighted gait pattern is assumed to be a true solution, so by comparing known suboptimal solutions virtual mass analysis can be used as a method to reject potential suggested biologic performance criteria.

4 Results

This chapter presents the gait parameters from the unloaded walking data, the adaptive loaded data, and the virtual non-adaptive loaded data. The adaptive loaded data is from walking at a self-selected speed while wearing a 5 kg mass attached to the right shin. The non-adaptive loaded data in contrast is generated by placing a 5 kg mass on the right shin during analysis using the normal unloaded walking kinematic data and recalculating the dynamics. The Wilcoxon rank sum test is performed to compare the adaptive loaded data and non-adaptive loaded data with the normal dataset. Confidence intervals and significance levels are presented for the comparisons.

4.1 Kinematic Gait Parameters

The kinematics of the lower body were examined in order to quantitatively verify the deviations in gait pattern due to the inertial load on the right leg. Thigh, knee, and ankle rotation angles and angular velocities were studied at various points throughout the gait cycle. Various maxima and minima of the angles for the thigh, knee, and ankle respectively were found, and the temporal parameters associated with the maxima/minima.

4.1.1 Ankle Kinematic Data

The ankle shows little variation kinematically due to the added mass. There was a decrease of 4° in peak swing plantarflexion. The results show a deviation of -2.2% of a gait cycle in the time at the peak mid-stance dorsiflexion. This result is consistent with other results of a general reduction in the stance phase by approximately 2% of the gait cycle. Additionally, the examination yielded deviations of -2.3% and -7.1% of the time at peak swing ankle plantarflexion and time at peak swing ankle dorsiflexion respectively. The deviation in time at which peak plantarflexion occurred is roughly the same as seen in the peak stance dorsiflexion and is consistent with a general shift in the timing of the stance phase of the gait cycle.

Data Type	Normal		Weighted		Normal vs. Weighted		
	Mean	Range	Mean	Range	P-Values	Est. Median Diff	95% Confidence Interval
Loading response peak ankle plantarflexion (deg)	80.60	10.98	80.13	13.57	0.557		
Terminal stance peak ankle dorsiflexion (deg)	99.84	7.86	100.81	10.45	0.322		
Swing peak ankle plantarflexion (deg)	68.15	21.68	73.30	20.73	0.020	3.95	1.64 ... 9.58
Swing peak ankle dorsiflexion (deg)	90.45	6.91	92.28	11.08	0.375		
Time at loading response peak ankle plantarflexion (% GC)	6.04	2.54	5.66	2.38	0.432		
Time at terminal stance peak ankle dorsiflexion (% GC)	47.52	8.76	45.31	8.80	0.004	-2.22	-2.98 ... -1.61
Time at swing peak ankle plantarflexion (% GC)	63.45	5.57	61.08	6.76	0.002	-2.29	-3.27 ... -1.67
Time at swing peak ankle dorsiflexion (% GC)	88.67	15.05	81.05	12.35	0.002	-7.05	-12.51 ... -2.79

Table 4.1.1 Ankle kinematic data for normal and right ankle loaded gait. The means and range for the ten subjects is presented. The p-value for the Wilcoxon rank sign test and the estimated median difference and 95% confidence interval on the median difference are presented. A positive estimated median difference indicates that the loaded case has a higher median.

4.1.2 Knee Kinematic Data

The peak mid-swing flexion angle is the only statistically significant change in the knee angle; the maximum flexion during swing for the loaded test is an on average 7.5° smaller than during the unperturbed normal walking test. An examination of the angular velocity of the knee produces some interesting results. During loading response flexion and mid-stance extension, the loaded study has a greater angular velocity than the normal study. However, during swing and pre-swing significantly lower angular velocities for the loaded data set are seen. There is a general change in the temporal parameters by approximately 2% of a gait cycle as described earlier. The time at toe off is an estimated 1.7% earlier for the loaded case as compared to the normal case.

Additionally, the time at terminal swing maximum extension is also deviated by approximately -1.9%. Thus, while the stance phase is compressed by 1.7%, the swing phase from toe off to maximum terminal swing extension is unchanged, i.e. the swing phase is only shifted in time and not compressed.

Table 4.1.2 Knee kinematic data for normal and right ankle loaded gait. Data mean and range over ten subjects is presented. The p-value for the Wilcoxon rank sign test and the estimated median difference and 95% confidence interval on the median difference are presented. A positive estimated median difference indicates that the loaded case has a higher median.

Data Type	Normal		Weighted		Normal vs. Weighted		
	Mean	Range	Mean	Range	P-Values	Est. Median Diff	95% Confidence Interval
Angles							
Knee angle at heelstrike (deg)	3.62	9.35	3.10	10.93	0.557		
Knee angle at toe off (deg)	31.59	16.30	31.17	17.71	0.557		
Mid-stance peak knee flexion (deg)	15.12	20.71	16.55	23.58	0.064		
Mid-swing peak knee flexion (deg)	56.17	13.69	48.37	22.30	0.002	-7.50	-11.32 ... -4.70
Terminal stance peak knee extension (deg)	0.98	15.67	0.54	13.94	0.375		
Terminal swing peak knee extension (deg)	2.29	8.34	1.09	8.98	0.322		
Angular Velocities							
Initial swing peak knee angular velocity (deg/s)	316.31	74.39	251.94	56.58	0.002	-58.65	-90.77 ... -44.76
Knee angular velocity at toe off (deg/s)	309.86	69.41	251.94	56.58	0.002	-52.61	-82.30 ... -41.18
Loading response peak knee angular velocity (deg/s)	132.85	115.36	151.69	127.59	0.037	23.32	1.02 ... 30.57
Mid-stance peak knee angular velocity (deg/s)	84.32	74.65	104.56	91.65	0.002	17.39	12.01 ... 30.38
Pre-swing peak knee angular velocity (deg/s)	310.90	69.41	255.96	70.50	0.002	-49.87	-80.53 ... -34.61
Swing peak knee extension angular velocity (deg/s)	341.17	49.02	287.39	131.19	0.006	-52.29	-83.64 ... -23.36
Temporal Parameters							
Time at initial swing peak knee angular velocity (% GC)	62.05	3.04	59.24	5.34	0.004	-3.19	-3.65 ... -1.62
Time at loading response peak knee angular velocity (% GC)	3.92	4.77	3.76	2.07	0.557		
Time at mid-stance peak knee angular velocity (% GC)	23.84	10.09	21.06	6.99	0.027	-2.95	-5.24 ... -0.58
Time at mid-stance peak knee flexion (% GC)	13.08	5.06	12.34	3.37	0.049	-0.75	-1.39 ... -0.07
Time at mid-swing peak knee flexion (% GC)	72.28	5.27	69.85	6.34	0.002	-2.42	-3.03 ... -1.76
Time at pre-swing peak knee angular velocity (% GC)	60.63	3.32	57.97	4.65	0.004	-2.84	-3.52 ... -1.94
Time at swing peak knee extension angular velocity (% GC)	85.69	6.87	84.56	10.34	0.084		
Time at terminal stance peak knee extension (% GC)	39.64	9.32	37.63	10.26	0.004	-2.07	-2.86 ... -1.22
Time at terminal swing peak knee extension (% GC)	97.63	3.80	95.76	3.84	0.002	-1.88	-2.55 ... -1.27
Time at toe off (% GC)	60.83	3.00	59.04	5.58	0.010	-1.74	-2.65 ... -0.79

4.1.3   Hip Kinematic Data

Similar to the kinematic analysis of the knee, there is only one significant large change in hip angle. The thigh angle at heel strike is 1.5° greater in the loaded test case than normal unloaded walking. In examination of the angular velocity at the hip, there is a significantly lower peak flexion angular velocity. The results from the kinematic analysis of the knee showed a similar reduction in angular velocities during the swing phase due to the added mass. Furthermore there was an increase in the peak extension angular velocity, and a decrease in the total range of angular velocity at the hip. All temporal parameters occurred earlier in the gait cycle by approximately 2-4%.

Data Type	Normal		Weighted		Normal vs. Weighted		
	Mean	Range	Mean	Range	P-Values	Est. Median Diff	95% Confidence Interval
Peak thigh extension (deg)	21.71	22.84	21.49	22.95	0.922		
Thigh angle at heelstrike (deg)	23.06	17.58	24.62	16.53	0.010	1.45	0.55 ... 2.52
Thigh angle at toe off (deg)	14.48	23.18	14.55	22.49	1.000		
Thigh angle range (deg)	46.24	18.89	46.71	15.50	0.375		
Range of thigh angular velocity (deg/s)	343.17	137.72	324.60	116.60	0.010	-18.65	-29.41 ... -7.53
Thigh extension peak angular velocity (deg/s)	130.80	59.45	143.91	73.35	0.004	12.53	7.08 ... 19.38
Thigh flexion peak angular velocity (deg/s)	213.06	74.21	181.65	60.98	0.002	-30.81	-43.20 ... -21.09
Time at peak thigh extension (% GC)	52.16	3.94	49.54	5.16	0.002	-2.56	-3.32 ... -2.03
Time at thigh extension peak angular velocity (% GC)	24.61	14.32	20.67	16.43	0.004	-3.94	-6.18 ... -1.84
Time at thigh flexion peak angular velocity (% GC)	66.35	3.42	63.83	4.78	0.002	-2.62	-3.36 ... -1.68

Table 4.1.3 Hip kinematic data for normal and right ankle loaded gait. Data mean and range over ten subjects is presented. The p-value for the Wilcoxon rank sign test and the estimated median difference and 95% confidence interval on the median difference are presented. A positive estimated median difference indicates that the loaded case has a higher median.

4.2   Whole Body Gait Parameters

This section examines the changes in total system gait parameters, e.g. parameters associated with the total body angular momentum, the derivative of total angular momentum, body torque, and system energy. The motivation for examining total system parameters such as this was to determine if any system parameters were invariant to the inertial disturbance.

4.2.1 Stride Parameters

No significant changes in stride time, stride length, step length, or self-selected walking speed were found. Walking speed was controlled in the experimental protocol, so this comparison indicates that the self-selected walking speed in the loaded condition was not statistically significantly different from the unloaded case.

Data Type	Normal		Weighted		Normal vs. Weighted		
						Median Est. Diff	
	Mean	Range	Mean	Range	P-Val	Val.	(% of norm)
Calculated Stride Time (s)	1.06	0.27	1.08	0.28	0.375		
Calculated Step Time (s)	0.41	0.09	0.44	0.12	*0.020*	*0.03*	*7.05*
Calculated Normalized Stride Length (m/m)	0.78	0.13	0.79	0.18	0.492		
Calculated Normalized Step Length (m/m)	0.38	0.06	0.39	0.13	0.160		
Calculated Walking speed (m/s)	1.29	0.35	1.27	0.32	0.375		

Table 4.2.1 Stride parameter Wilcoxon rank sign test comparison. Stride and Step length have been normalized with respect to subject height.

4.2.2 Body Center of Mass Motion Parameters

The motion of the body center of mass was fitted using a linear least squares regression method and then the residuals from this regression were analyzed instead of the actual motion of the body center of mass. The impetus for this type of analysis is that examining the residuals will account for any errors introduced into the calculations from a small error in the orientation of the motion capture system. In particular, the motion capture system shows that subjects walk down slightly as they travel along the walkway in the motion lab. Examining the unadjusted data to determine the variance in the vertical position of the body center of mass would produce erroneous results.

The coronal root mean square distance of the body center of mass away from the linear fit is the smallest for the unloaded walking case. The true loaded case has the second smallest RMS distance, with the loaded kinematic case and the non-adaptive mass case both having larger deviations from the linear fit. The two synthetic test cases, the non-adaptive loaded case and the loaded kinematics case, are both greatly higher than normal by 187% and 105% respectively. That is, that a true biological walking pattern has less deviation in the forward progression than either a virtually perturbed pattern or the calculation of the loaded kinematics body center of mass when the 5 kg mass was not included in the BCOM calculation. In addition to the coronal RMS

deviation from the linear fit, there is greater amplitude of deviation from the transverse plane of the body center of mass of the loaded case versus the normal case. Similarly to position deviation, there is a greater velocity RMS deviation from the coronal plane of the body center of mass, with the normal walking case having the smallest RMS velocity deviation, the true loaded case having the second smallest RMS velocity deviation, and the two synthetic cases both having higher RMS values.

Table 4.2.2 Body center of mass parameter Wilcoxon rank sign test comparisons. Position data has been normalized with subject height. Velocity data has been normalized with subject height and gait frequency.

Data Type	Normal Mean	Normal Range	Weighted Mean	Weighted Range	Virtual Mass Mean	Virtual Mass Range	Weighted Kin. Mean	Weighted Kin. Range
Position								
Calculated BCOM Travel during Single Support (cm/m)	60.16	9.44	60.71	13.77	60.69	9.51	60.19	13.81
Calculated BCOM Travel during Double Support (cm/m)	18.25	4.26	18.32	5.37	17.73	4.38	18.85	5.41
Sagittal RMS of distance of BCOM away from linear fit (cm/m)	0.52	0.69	0.50	0.33	0.49	0.68	0.55	0.34
Coronal RMS of distance of BCOM away from linear fit (cm/m)	0.29	0.24	0.43	0.32	0.84	0.68	0.59	0.42
Transverse RMS of distance of BCOM away from linear fit (cm/m)	0.62	0.48	0.67	0.50	0.60	0.40	0.69	0.54
Sagittal amplitude of distance of BCOM away from linear fit (cm/m)	1.06	1.42	1.02	0.61	0.99	1.40	1.13	0.62
Coronal amplitude of distance of BCOM away from linear fit (cm/m)	0.52	0.42	0.84	0.62	1.29	0.98	1.18	1.12
Transverse amplitude of distance of BCOM away from linear fit (cm/m)	1.03	0.86	1.17	1.03	1.03	0.78	1.17	1.06
Velocities								
Sagittal RMS velocity of BCOM deviation from mean path (cms/ms)	4.59	5.37	4.65	3.35	4.24	5.28	5.17	3.43
Coronal RMS velocity of BCOM deviation from mean path (cms/ms)	3.64	3.01	4.49	3.80	5.74	3.47	5.77	5.03
Transverse RMS velocity of BCOM deviation from mean path (cms/ms)	7.86	6.26	8.28	6.48	7.64	5.61	8.66	6.82
Sagittal velocity amplitude of BCOM deviation from mean path (cms/ms)	7.67	8.56	7.90	5.17	7.02	7.77	8.82	5.27
Coronal velocity amplitude of BCOM deviation from mean path (cms/ms)	6.10	4.60	8.03	8.36	8.75	4.49	10.39	9.93
Transverse velocity amplitude of BCOM deviation from mean path (cms/ms)	11.79	9.95	12.42	10.81	11.54	8.58	13.17	11.16

Data Type	Normal Mean	Normal vs. Weighted P-Val	Normal vs. Weighted Median Est. Diff Val.	Normal vs. Weighted Median Est. Diff (% of norm)	Normal vs. Virtual Mass P-Val	Normal vs. Virtual Mass Median Est. Diff Val.	Normal vs. Virtual Mass Median Est. Diff (% of norm)	Normal vs. Weighted Kin. P-Val	Normal vs. Weighted Kin. Median Est. Diff Val.	Normal vs. Weighted Kin. Median Est. Diff (% of norm)
Position										
Calculated BCOM Travel during Single Support (cm/m)	60.16	0.557			*0.002*	*0.52*	*0.86*	1.000		
Calculated BCOM Travel during Double Support (cm/m)	18.25	0.695			*0.002*	*-0.52*	*-2.84*	*0.004*	*0.60*	*3.27*
Sagittal RMS of distance of BCOM away from linear fit (cm/m)	0.52	0.770			*0.002*	*-0.03*	*-6.48*	0.232		
Coronal RMS of distance of BCOM away from linear fit (cm/m)	0.29	*0.004*	*0.15*	*50.20*	*0.002*	*0.54*	*186.50*	*0.002*	*0.30*	*104.88*
Transverse RMS of distance of BCOM away from linear fit (cm/m)	0.62	0.193			*0.027*	*-0.02*	*-3.73*	*0.027*	*0.07*	*11.30*
Sagittal amplitude of distance of BCOM away from linear fit (cm/m)	1.06	1.000			*0.002*	*-0.07*	*-6.80*	0.193		
Coronal amplitude of distance of BCOM away from linear fit (cm/m)	0.52	*0.002*	*0.31*	*60.23*	*0.002*	*0.73*	*140.07*	*0.002*	*0.65*	*124.95*
Transverse amplitude of distance of BCOM away from linear fit (cm/m)	1.03	*0.027*	*0.15*	*14.78*	0.846			*0.027*	*0.15*	*14.58*
Velocities										
Sagittal RMS velocity of BCOM deviation from mean path (cms/ms)	4.59	0.770			*0.002*	*-0.35*	*-7.61*	*0.027*	*0.64*	*13.93*
Coronal RMS velocity of BCOM deviation from mean path (cms/ms)	3.64	*0.006*	*0.87*	*23.79*	*0.002*	*2.00*	*55.02*	*0.002*	*2.12*	*58.25*
Transverse RMS velocity of BCOM deviation from mean path (cms/ms)	7.86	0.160			*0.020*	*-0.22*	*-2.75*	*0.049*	*0.79*	*10.00*
Sagittal velocity amplitude of BCOM deviation from mean path (cms/ms)	7.67	0.695			*0.002*	*-0.64*	*-8.36*	*0.027*	*1.23*	*16.07*
Coronal velocity amplitude of BCOM deviation from mean path (cms/ms)	6.10	*0.002*	*1.73*	*28.28*	*0.002*	*2.73*	*44.74*	*0.002*	*4.11*	*67.34*
Transverse velocity amplitude of BCOM deviation from mean path (cms/ms)	11.79	0.275			0.131			*0.027*	*1.45*	*12.26*

4.2.3   BCOM and System Energy Parameters

In the absence of true metabolic rate measurements that evaluate the rate of oxygen consumption, the main way of estimating gait energy efficiency is by examining the transfer of mechanical energy in the system. Using the normal unloaded walking kinematics, a load was placed on the right leg in the analysis and the dynamics recalculated generating data referred to as the non-adaptive loaded case. The non-adaptive loaded case had lower gait efficiencies, higher powers, and higher positive works than both the adaptive loaded and normal test cases. For the non-adaptive loaded case: the BCOM energy recovery was 32% lower, the RMS power to move the BCOM was 66% greater, and the positive work to move the BCOM was 51% greater than normal. Conversely to the non-adaptive loaded case, where all parameters were significantly worse, the loaded kinematics case had significantly higher gait efficiencies in some instances. The body center of mass energy recovery for the loaded kinematics case was 8% greater than normal. All energy parameters for the adaptive loaded case were significantly poorer than normal; the BCOM energy recovery was 13% lower, the RMS power to move the BCOM was 22% greater, and the positive work to move the BCOM was 22% greater than normal.

Table 4.2.3 Body center of mass and system energy parameter Wilcoxon rank sign test comparisons. Calculated power parameters have been normalized by $M_{tot} g^{3/2} H^{1/2}$. Calculated work parameters have been normalized by $M_{tot} g H$.

	Data Type	Normal		Weighted		Virtual Mass		Weighted Kin.	
		Mean	Range	Mean	Range	Mean	Range	Mean	Range
Efficiency	BCOM Energy Percent Signal Cancellation (%)	89.12	19.47	77.13	33.41	54.48	36.61	88.14	15.40
	BCOM Energy Recovery (%)	65.48	30.26	56.36	32.45	44.40	30.86	70.94	15.88
	BCOM Potential-Kinetic Energy Recovery (%)	65.56	30.17	56.61	30.41	45.01	31.20	70.96	16.47
	Total System Energy Recovery (%)	35.94	33.48	27.04	29.68	21.26	21.61	47.03	30.71
Power	Normalized RMS Total Power	0.036	0.022	0.046	0.031	0.058	0.037	0.035	0.023
	Normalized RMS BCOM Power	0.020	0.012	0.025	0.016	0.034	0.022	0.022	0.021
	Normalized RMS External Power	0.020	0.012	0.025	0.016	0.034	0.022	0.022	0.021
	Normalized RMS Internal Power	0.020	0.014	0.027	0.020	0.030	0.021	0.020	0.017
Work	Normalized System Positive Work	0.038	0.022	0.049	0.026	0.057	0.036	0.035	0.019
	Normalized BCOM Positive Work	0.021	0.012	0.026	0.014	0.033	0.017	0.021	0.017
	Normalized External Positive Work	0.021	0.012	0.026	0.014	0.033	0.017	0.021	0.017
	Normalized Internal Positive Work	0.020	0.011	0.028	0.019	0.028	0.013	0.020	0.015

	Data Type	Normal	Normal vs. Weighted			Normal vs. Virtual Mass			Normal vs.Weighted Kin.		
		Mean	P-Val	Val.	(% of norm)	P-Val	Val.	(% of norm)	P-Val	Val.	(% of norm)
Efficiency	BCOM Energy Percent Signal Cancellation (%)	89.12	0.002	-0.11	-12.47	0.002	-0.35	-39.13	0.322		
	BCOM Energy Recovery (%)	65.48	0.002	-0.09	-13.20	0.002	-0.21	-31.51	0.006	0.05	7.84
	BCOM Potential-Kinetic Energy Recovery (%)	65.56	0.002	-0.09	-13.04	0.002	-0.20	-30.59	0.006	0.05	7.75
	Total System Energy Recovery (%)	35.94	0.002	-0.09	-25.20	0.002	-0.14	-40.19	0.002	0.11	30.64
Power	Normalized RMS Total Power	0.036	0.002	0.010	28.43	0.002	0.022	61.90	0.695		
	Normalized RMS BCOM Power	0.020	0.004	0.004	22.24	0.002	0.013	66.43	0.375		
	Normalized RMS External Power	0.020	0.004	0.004	22.24	0.002	0.013	66.43	0.375		
	Normalized RMS Internal Power	0.020	0.002	0.007	35.31	0.002	0.009	47.98	0.625		
Work	Normalized System Positive Work	0.038	0.002	0.011	29.56	0.002	0.018	48.81	0.105		
	Normalized BCOM Positive Work	0.021	0.004	0.005	21.81	0.002	0.011	51.11	1.000		
	Normalized External Positive Work	0.021	0.004	0.005	21.81	0.002	0.011	51.11	1.000		
	Normalized Internal Positive Work	0.020	0.002	0.008	39.49	0.002	0.008	41.49	1.000		

4.2.4   System Angular Momentum Parameters

The Wilcoxon rank sign test comparison of the normal and loaded datasets revealed significant increases of every momentum parameter; the maximum sagittal normalized spin was 269% greater, the sagittal RMS normalized spin was 160% greater, and the coronal RMS normalized spin was 96% greater than normal. A similar result was found when the normal case was compared to the adaptive loaded case; the maximum sagittal normalized spin was 287% greater, the sagittal RMS normalized spin was 175% greater, and the coronal RMS normalized spin was only 51% greater than normal. Calculating the total angular momentum for the loaded kinematics, i.e. angular momentum for the body not including the 5 kg added mass, revealed only three significantly different parameters all relating to the coronal plane. There were significant increases of 35% in maximum coronal normalized spin, 19% in minimum coronal normalized spin, and 37% coronal RMS normalized spin.

Table 4.2.4 System angular momentum parameter Wilcoxon rank sign test comparisons. Angular momentum values have been normalized with subject height, mass, and walking speed.

Data Type	Normal		Weighted		Virtual Mass		Weighted Kin.	
	Mean	Range	Mean	Range	Mean	Range	Mean	Range
Maximum normalized spin	0.029	0.011	0.060	0.025	0.062	0.032	0.030	0.013
Sagittal maximum normalized spin	0.015	0.007	0.058	0.028	0.061	0.032	0.016	0.010
Coronal maximum normalized spin	0.011	0.007	0.021	0.012	0.016	0.008	0.015	0.010
Transverse maximum normalized spin	0.005	0.005	0.010	0.008	0.010	0.008	0.005	0.003
Sagittal minimum normalized spin	0.026	0.013	0.049	0.014	0.048	0.015	0.027	0.015
Coronal minimum normalized spin	0.011	0.014	0.019	0.012	0.017	0.016	0.013	0.010
Transverse minimum normalized spin	0.005	0.006	0.007	0.007	0.007	0.006	0.005	0.008
RMS normalized spin	0.015	0.006	0.037	0.013	0.038	0.015	0.015	0.004
Sagittal RMS normalized spin	0.013	0.007	0.035	0.013	0.037	0.015	0.013	0.006
Coronal RMS normalized spin	0.005	0.006	0.011	0.006	0.008	0.007	0.008	0.005
Transverse RMS normalized spin	0.004	0.005	0.007	0.004	0.006	0.006	0.003	0.004

Data Type	Normal	Normal vs. Weighted			Normal vs. Virtual Mass			Normal vs. Weighted Kin.		
	Mean	P-Val	Median Est. Diff Val.	(% of norm)	P-Val	Median Est. Diff Val.	(% of norm)	P-Val	Median Est. Diff Val.	(% of norm)
Maximum normalized spin	0.029	0.002	0.030	104.46	0.002	0.032	113.04	0.193		
Sagittal maximum normalized spin	0.015	0.002	0.041	269.14	0.002	0.044	286.84	0.695		
Coronal maximum normalized spin	0.011	0.002	0.009	83.84	0.002	0.005	46.28	0.002	0.004	34.96
Transverse maximum normalized spin	0.005	0.002	0.005	93.23	0.002	0.005	90.90	0.492		
Sagittal minimum normalized spin	0.026	0.002	0.023	89.26	0.002	0.022	83.58	0.770		
Coronal minimum normalized spin	0.011	0.002	0.008	76.75	0.002	0.006	51.74	0.004	0.002	18.81
Transverse minimum normalized spin	0.005	0.002	0.002	37.54	0.002	0.002	36.24	0.160		
RMS normalized spin	0.015	0.002	0.021	141.19	0.002	0.022	148.00	0.922		
Sagittal RMS normalized spin	0.013	0.002	0.021	159.90	0.002	0.023	174.85	0.193		
Coronal RMS normalized spin	0.005	0.002	0.005	95.59	0.002	0.003	50.83	0.002	0.002	37.40
Transverse RMS normalized spin	0.004	0.002	0.003	79.93	0.002	0.003	71.86	0.105		

4.2.5   System Momentum Cancellation Parameters

Normal unloaded walking exhibits angular momentum percentage signal cancellations of 95%, 57%, and 89% in the sagittal, coronal, and transverse planes respectively. In the sagittal and transverse planes, where the highest degree of signal cancellation is found, there is a reduction of 10% and 5% in angular momentum signal cancellation respectively for the adaptive loaded data set. For the non-adaptive loaded data set, there is a reduction of 12% and 10% in the sagittal and transverse planes respectively. When examining the loaded kinematics dataset, there was an increase of 1% and 4% in the sagittal and transverse planes and a decrease of 20% total angular momentum signal cancellation versus normal.

The linear momentum percent signal cancellation is 96% in the coronal plane for normal unloaded walking, however there were no significant differences between the normal and adaptive loaded walking dataset. The non-adaptive loaded and adaptive loaded kinematics datasets have lower percentages linear momentum signal cancellation in the coronal plane by an estimated 2% and 5% respectively.

Table 4.2.5 System angular and linear momentum cancellation parameter Wilcoxon rank sign test comparisons. Percent signal cancellation methodology is outlined in section 3.8.5.3.

Data Type	Normal Mean	Normal Range	Weighted Mean	Weighted Range	Virtual Mass Mean	Virtual Mass Range	Weighted Kin. Mean	Weighted Kin. Range
Angular								
Sagittal total signal cancellation (%)	95.24	3.78	85.10	6.99	83.35	9.15	96.10	2.79
Coronal total signal cancellation (%)	57.12	53.50	38.55	23.78	46.24	42.10	45.90	30.37
Transverse total signal cancellation (%)	89.08	22.79	85.01	22.97	80.71	28.08	93.03	19.48
Sagittal upper-lower body signal cancellation (%)	14.81	18.75	4.41	4.20	2.74	2.23	30.79	43.76
Coronal upper-lower body signal cancellation (%)	16.12	34.18	4.72	6.61	7.50	12.51	8.17	21.53
Transverse upper-lower body signal cancellation (%)	86.93	27.80	81.80	27.86	76.61	34.48	91.66	23.79
Sagittal right-left body signal cancellation (%)	94.22	4.64	83.22	7.75	81.33	9.40	95.22	3.31
Coronal right-left body signal cancellation (%)	29.08	43.86	13.36	13.64	20.22	33.24	16.99	22.20
Transverse right-left body signal cancellation (%)	33.15	59.41	24.04	34.64	18.41	33.38	45.97	57.92
Sagittal major body segments signal cancellation (%)	94.27	4.60	83.28	7.73	81.49	9.33	95.25	3.29
Coronal major body segments signal cancellation (%)	37.92	52.78	20.50	21.92	28.05	41.87	26.68	30.50
Transverse major body segments signal cancellation (%)	87.53	26.13	82.45	26.38	77.58	32.26	91.95	22.67
Linear								
Sagittal linear momentum total signal cancellation (%)	28.69	36.46	40.77	36.67	37.53	40.25	29.77	28.68
Coronal linear momentum total signal cancellation (%)	95.87	5.20	96.17	5.09	93.34	7.54	91.09	11.70
Transverse linear momentum total signal cancellation (%)	33.64	26.94	41.52	25.56	43.87	25.58	31.25	20.45

Data Type	Normal Mean	Normal vs. Weighted P-Val	Normal vs. Weighted Median Est. Diff Val.	Normal vs. Weighted Median Est. Diff (% of norm)	Normal vs. Virtual Mass P-Val	Normal vs. Virtual Mass Median Est. Diff Val.	Normal vs. Virtual Mass Median Est. Diff (% of norm)	Normal vs. Weighted Kin. P-Val	Normal vs. Weighted Kin. Median Est. Diff Val.	Normal vs. Weighted Kin. Median Est. Diff (% of norm)
Angular										
Sagittal total signal cancellation (%)	95.24	0.002	-9.94	-10.44	0.002	-11.54	-12.11	0.002	0.91	0.95
Coronal total signal cancellation (%)	57.12	0.004	-18.78	-32.88	0.004	-10.04	-17.57	0.010	-11.32	-19.82
Transverse total signal cancellation (%)	89.08	0.049	-4.02	-4.51	0.002	-8.66	-9.73	0.014	3.45	3.88
Sagittal upper-lower body signal cancellation (%)	14.81	0.002	-9.96	-67.27	0.002	-12.07	-81.46	0.002	14.86	100.33
Coronal upper-lower body signal cancellation (%)	16.12	0.002	-11.54	-71.60	0.002	-8.61	-53.43	0.010	-7.90	-49.05
Transverse upper-lower body signal cancellation (%)	86.93	0.049	-4.58	-5.27	0.002	-10.62	-12.22	0.014	4.25	4.89
Sagittal right-left body signal cancellation (%)	94.22	0.002	-10.78	-11.44	0.002	-12.70	-13.48	0.010	1.01	1.07
Coronal right-left body signal cancellation (%)	29.08	0.010	-15.36	-52.84	0.004	-8.98	-30.88	0.020	-12.46	-42.84
Transverse right-left body signal cancellation (%)	33.15	0.020	-8.51	-25.66	0.002	-13.48	-40.64	0.004	12.16	36.67
Sagittal major body segments signal cancellation (%)	94.27	0.002	-10.76	-11.41	0.002	-12.45	-13.21	0.010	0.99	1.05
Coronal major body segments signal cancellation (%)	37.92	0.004	-17.01	-44.86	0.002	-9.51	-25.07	0.004	-10.38	-27.37
Transverse major body segments signal cancellation (%)	87.53	0.049	-4.89	-5.59	0.002	-10.26	-11.72	0.014	3.99	4.56
Linear										
Sagittal linear momentum total signal cancellation (%)	28.69	0.004	13.15	45.82	0.002	8.68	30.26	0.770		
Coronal linear momentum total signal cancellation (%)	95.87	0.375			0.010	-2.29	-2.39	0.002	-4.64	-4.84
Transverse linear momentum total signal cancellation (%)	33.64	0.004	7.31	21.72	0.002	10.17	30.22	0.084		

4.2.6   System Net External Torque Parameters

There were significant differences between the normal and adaptive loaded dataset and there were significant difference between the normal and non-adaptive loaded dataset. Without exception all peak torque and root mean torque values in the adaptive loaded set were significantly greater than the normal case. The RMS normalized body torque in the sagittal, coronal, and transverse planes for the adaptive loaded dataset was an estimated 75%, 71%, and 70% greater than normal respectively. The non-adaptive loaded dataset when compared to normal had increases of 98%, 58%, and 58% of RMS normalized body torque in the sagittal, coronal, and transverse planes. The loaded kinematics case had a decrease of 10% in the sagittal plane, but increases of 16% and 15% in the coronal and transverse planes of RMS normalized body torque.

Table 4.2.6 System net external torque parameter Wilcoxon rank sign test comparisons. Net external torque is the time derivative of total system angular momentum.

Data Type	Normal		Weighted		Virtual Mass		Weighted Kin.	
	Mean	Range	Mean	Range	Mean	Range	Mean	Range
Maximum normalized body torque	0.43	0.24	0.83	0.33	1.06	0.35	0.45	0.26
Maximum normalized sagittal body torque	0.31	0.13	0.63	0.23	0.61	0.18	0.31	0.28
Maximum normalized coronal body torque	0.12	0.07	0.21	0.08	0.22	0.08	0.14	0.05
Maximum normalized transverse body torque	0.06	0.07	0.11	0.08	0.10	0.07	0.07	0.06
Minimum normalized sagittal body torque	0.41	0.24	0.80	0.34	1.04	0.38	0.41	0.28
Minimum normalized coronal body torque	0.13	0.08	0.22	0.15	0.20	0.11	0.17	0.15
Minimum normalized transverse body torque	0.07	0.06	0.12	0.12	0.11	0.06	0.09	0.10
RMS normalized body torque	0.20	0.07	0.36	0.10	0.40	0.12	0.19	0.07
RMS normalized sagittal body torque	0.19	0.09	0.33	0.12	0.38	0.13	0.17	0.08
RMS normalized coronal body torque	0.06	0.04	0.11	0.05	0.10	0.04	0.07	0.04
RMS normalized transverse body torque	0.03	0.02	0.05	0.03	0.05	0.02	0.03	0.03

Data Type	Normal	Normal vs. Weighted			Normal vs. Virtual Mass			Normal vs.Weighted Kin.		
	Mean	P-Val	Median Est. Diff Val.	(% of norm)	P-Val	Median Est. Diff Val.	(% of norm)	P-Val	Median Est. Diff Val.	(% of norm)
Maximum normalized body torque	0.43	0.002	0.38	88.77	0.002	0.62	142.81	0.492		
Maximum normalized sagittal body torque	0.31	0.002	0.32	101.30	0.002	0.29	94.42	0.695		
Maximum normalized coronal body torque	0.12	0.002	0.09	68.80	0.002	0.09	72.47	0.037	0.01	8.50
Maximum normalized transverse body torque	0.06	0.002	0.04	68.43	0.002	0.04	54.35	0.084		
Minimum normalized sagittal body torque	0.41	0.002	0.38	90.83	0.002	0.61	148.32	0.770		
Minimum normalized coronal body torque	0.13	0.002	0.09	66.81	0.002	0.06	47.43	0.037	0.03	24.97
Minimum normalized transverse body torque	0.07	0.002	0.05	70.76	0.002	0.04	51.34	0.006	0.01	16.41
RMS normalized body torque	0.20	0.002	0.15	75.08	0.002	0.19	92.88	0.027	-0.01	-5.30
RMS normalized sagittal body torque	0.19	0.002	0.14	75.36	0.002	0.18	98.21	0.006	-0.02	-9.75
RMS normalized coronal body torque	0.06	0.002	0.04	70.72	0.002	0.04	58.07	0.010	0.01	16.30
RMS normalized transverse body torque	0.03	0.002	0.02	70.18	0.002	0.02	58.43	0.014	0.00	14.48

4.3   Kinetic Gait Parameters

The torques and powers at the right hip, knee, and ankle were calculated; however the method of recalculating the dynamics of the normal unloaded walking dataset with a mass on the right shin to form the non-adaptive loaded dataset can only be used to determine parameters during the swing phase of the right leg due to the absence of ground reaction force data. During double support the distribution of total ground reaction force between right and left legs is an indeterminate problem. Thus, for any synthetic walking case where the actual ground reaction force is absent, it is not possible to determine the reaction torques. This problem was examined in some detail to determine if an invariant load transfer function existed that could be used to project the net ground reaction force to left and right leg components during double support, however none was found. Regardless, since the added has maximal acceleration during swing, examination of reaction torques and powers during swing can be a useful tool.

Without exception, in the comparison of the adaptive loaded data set, all significantly different kinetic parameters were greater than normal. The knee peak flexion moment during terminal swing, the principal moment responsible for the deceleration of the shank prior to initial contact, for the adaptive loaded case is an estimated 93% greater than normal. Furthermore, the peak knee extension moment during initial swing for the adaptive loaded case is 72% greater than normal unloaded walking. The peak knee power absorption during initial and terminal swing for the adaptive loaded case was an estimated 37% and 52% greater than normal. The non-adaptive loaded case also shows significant increases. The peak knee extension and flexion moment during initial and terminal swing for the non-adaptive loaded dataset were 46% and 196% greater than normal respectively. Furthermore, the peak knee power absorption during the initial and terminal swing was an estimated 35% and 198% greater than during normal unloaded walking. The loaded kinematics comparison found decreases of 41% peak knee flexion moment and 48% peak knee power absorption during terminal swing versus normal.

Similar results were found in the analysis of the reaction torque and power at the hip. The peak hip flexion and extension moment during swing for the adaptive loaded case were an estimated 121% and 108% greater than normal. The non-adaptive case had peak hip flexion and extension moments during swing that were 128% and 227%

greater than normal respectively. The loaded kinematics dataset comparison found a decrease of 50% in peak hip extension moment during swing versus normal.

Table 4.3.1 Kinetic gait parameter means and ranges for knee, hip, and ankle for four weighting conditions. Calculated torque and power is normalized by subject height and mass. Only stance parameters for synthetic cases included.

Data Type	Normal Mean	Normal Range	Weighted Mean	Weighted Range	Virtual Mass Mean	Virtual Mass Range	Weighted Kin. Mean	Weighted Kin. Range
Peak Knee Flexion Moment During Loading Response (Nm/kgm)	0.22	0.27	0.30	0.29	..	..	..	..
Peak Knee Extension Moment During Mid-Stance (Nm/kgm)	0.22	0.30	0.30	0.42	..	..	..	..
Peak Knee Flexion Moment During Terminal Stance (Nm/kgm)	0.23	0.26	0.23	0.25	..	..	..	..
Peak Knee Extension Moment During Initial Swing (Nm/kgm)	0.07	0.06	0.12	0.14	0.10	0.11	0.08	0.07
Peak Knee Flexion Moment During Terminal Swing (Nm/kgm)	0.12	0.09	0.23	0.12	0.36	0.22	0.07	0.06
Peak Knee Power Generation During Loading Response (W/kgm)	0.38	0.46	0.64	0.67	..	..	..	..
Peak Knee Power Absorption During Loading Response (W/kgm)	0.30	0.58	0.44	0.88	..	..	..	..
Peak Knee Power Generation During Mid-Stance (W/kgm)	0.20	0.47	0.24	0.62	..	..	..	..
Peak Knee Power Absorption During Terminal Stance (W/kgm)	0.16	0.26	0.16	0.22	..	..	..	..
Peak Knee Power Generation During Pre-Swing	0.22	0.44	0.25	0.42	..	..	..	..
Peak Knee Power Absorption During Initial Swing (W/kgm)	0.39	0.33	0.55	0.57	0.53	0.68	0.36	0.28
Peak Knee Power Generation During Mid-Swing (W/kgm)	0.03	0.20	0.01	0.04	0.01	0.08	0.03	0.11
Peak Knee Power Absorption During Terminal Swing (W/kgm)	0.36	0.45	0.56	0.51	1.12	1.38	0.16	0.18
Peak Hip Flexion Moment During Stance (Nm/kgm)	0.49	0.56	0.53	0.53	..	..	..	..
Peak Hip Extension Moment During Stance (Nm/kgm)	0.45	0.50	0.68	0.34	..	..	..	..
Peak Hip Flexion Moment During Swing (Nm/kgm)	0.18	0.05	0.39	0.27	0.41	0.30	0.17	0.09
Peak Hip Extension Moment During Swing (Nm/kgm)	0.25	0.16	0.53	0.48	0.83	0.45	0.12	0.15
Peak Hip Power Generation During Loading Response (W/kgm)	0.35	0.38	0.49	0.47	..	..	..	..
Peak Hip Power Absorption During Stance (W/kgm)	0.39	0.47	0.44	0.71	..	..	..	..
Peak Hip Power Generation During Pre-Swing (W/kgm)	0.44	0.28	0.86	0.51	..	..	..	..
Peak Hip Power Generation During Initial Swing (W/kgm)	0.62	0.44	1.09	1.02	1.51	1.54	0.46	0.31
Peak Hip Power Absorption During Terminal Swing (W/kgm)	0.09	0.12	0.21	0.35	0.27	0.49	0.08	0.08
Peak Ankle PlantarFlexion Moment During Loading Response (Nm/kgm)	0.09	0.12	0.13	0.17	..	..	..	..
Peak Ankle DorsiFlexion Moment During Stance (Nm/kgm)	0.92	0.28	0.98	0.28	..	..	..	..
Peak Ankle Power Absorption During Loading Response (W/kgm)	0.19	0.30	0.34	0.38	..	..	..	..
Peak Ankle Power Absorption During Terminal Stance (W/kgm)	0.63	0.52	0.67	0.46	..	..	..	..
Peak Ankle Power Generation During Pre-Swing (W/kgm)	2.34	2.03	2.50	2.12	..	..	..	..

Table 4.3.2 Kinetic gait parameter Wilcoxon rank sign test comparisons for the knee, hip, and ankle under four weighting conditions. Calculated torque and power is normalized by subject height and mass.

	Data Type	Normal Mean	Normal vs. Weighted			Normal vs. Virtual Mass			Normal vs. Weighted Kin.		
			P-Val	Median Est. Diff		P-Val	Median Est. Diff		P-Val	Median Est. Diff	
				Val.	(% of norm)		Val.	(% of norm)		Val.	(% of norm)
Knee	Peak Knee Flexion Moment During Loading Response (Nm/kgm)	0.22	0.014	0.08	36.02	..			..		
	Peak Knee Extension Moment During Mid-Stance (Nm/kgm)	0.22	0.002	0.07	33.23	..			..		
	Peak Knee Flexion Moment During Terminal Stance (Nm/kgm)	0.23	0.922			..			..		
	Peak Knee Extension Moment During Initial Swing (Nm/kgm)	0.07	0.002	0.05	71.93	0.004	0.03	45.97	0.084		
	Peak Knee Flexion Moment During Terminal Swing (Nm/kgm)	0.12	0.002	0.11	93.22	0.002	0.24	195.96	0.002	-0.05	-41.49
	Peak Knee Power Generation During Loading Response (W/kgm)	0.38	0.002	0.27	73.04	..			..		
	Peak Knee Power Absorption During Loading Response (W/kgm)	0.30	0.002	0.11	36.73	..			..		
	Peak Knee Power Generation During Mid-Stance (W/kgm)	0.20	0.232			..			..		
	Peak Knee Power Absorption During Terminal Stance (W/kgm)	0.16	0.846			..			..		
	Peak Knee Power Generation During Pre-Swing	0.22	0.492			..			..		
	Peak Knee Power Absorption During Initial Swing (W/kgm)	0.39	0.004	0.14	36.70	0.020	0.14	35.01	0.375		
	Peak Knee Power Generation During Mid-Swing (W/kgm)	0.03	0.557			0.375			1.000		
	Peak Knee Power Absorption During Terminal Swing (W/kgm)	0.36	0.002	0.19	52.40	0.002	0.72	198.14	0.002	-0.18	-48.20
Hip	Peak Hip Flexion Moment During Stance (Nm/kgm)	0.49	0.037	0.03	6.40	..			..		
	Peak Hip Extension Moment During Stance (Nm/kgm)	0.45	0.002	0.23	50.39	..			..		
	Peak Hip Flexion Moment During Swing (Nm/kgm)	0.18	0.002	0.21	121.45	0.002	0.23	127.61	0.275		
	Peak Hip Extension Moment During Swing (Nm/kgm)	0.25	0.002	0.27	108.08	0.002	0.57	226.62	0.002	-0.13	-50.48
	Peak Hip Power Generation During Loading Response (W/kgm)	0.35	0.010	0.14	39.38	..			..		
	Peak Hip Power Absorption During Stance (W/kgm)	0.39	0.375			..			..		
	Peak Hip Power Generation During Pre-Swing (W/kgm)	0.44	0.002	0.41	92.04	..			..		
	Peak Hip Power Generation During Initial Swing (W/kgm)	0.62	0.002	0.47	75.42	0.002	0.85	135.44	0.006	-0.17	-27.80
	Peak Hip Power Absorption During Terminal Swing (W/kgm)	0.09	0.049	0.12	126.48	0.010	0.17	185.18	0.105		
Ankle	Peak Ankle PlantarFlexion Moment During Loading Response (Nm/kgm)	0.09	0.002	0.04	43.28	..			..		
	Peak Ankle DorsiFlexion Moment During Stance (Nm/kgm)	0.92	0.020	0.06	5.99	..			..		
	Peak Ankle Power Absorption During Loading Response (W/kgm)	0.19	0.002	0.16	83.86	..			..		
	Peak Ankle Power Absorption During Terminal Stance (W/kgm)	0.63	0.557			..			..		
	Peak Ankle Power Generation During Pre-Swing (W/kgm)	2.34	0.322			..			..		

5 Discussion

In the control of humanoid robotics, advanced prostheses, and functional neuromuscular stimulation there is a need for biologically realistic target gait trajectories. Synthesis of target trajectories can be a complex computationally-intensive process that is not geared towards online, on demand applications. Thus, for near real-time synthesis of biologically realistic gait trajectories, a simpler, reduced-order methodology is necessary. It is a generally accepted principle that biologic gait patterns emerge from the optimization of some cost objective function of the motor control system (Nubar & Contini 1961, Chow & Jacobson 1971). Furthermore there is a number of possible performance criteria that can result in biologically realistic gait patterns (Marshall et al. 1989). It was hypothesized that the true nature of the constitution of the biologic performance criterion might be elucidated by perturbing human subjects while walking and quantitatively measuring the reorganization of gait. Towards the development of a reduced order method to generate biologically realistic gait kinematics, ten healthy subjects were perturbed with an inertial load of 5 kg worn on the right shin. Two chief comparisons were used to measure gait changes due to the inertial load and the effect of these deviations. Data from the trials with the load were compared to those without to determine the existence of invariant quantities. Secondly, the adaptive loaded dataset was compared to the kinematics of the unloaded normal dataset with the dynamics recalculated with a 5 kg mass virtually placed on the right shin of the normal data. The

non-adaptive virtually loaded case served as basis of comparison to determine the effect of gait reorganization. I assumed that the non-adaptive loaded symmetric gait patterns with the virtual mass served as starting point for the motor control system, and any deviation from normal would be an effort to minimize the biologic performance criterion. I hypothesized that there would be a significant change in gait kinematics to reflect the general gait reorganization and that these changes would induce an increase in walking efficiency, decrease in work to move the body center of mass, not change the motion of the center of mass significantly, and reduce joint torques. This chapter reviews the individual analyses and their significance in rejection or acceptance of these hypotheses.

5.1   Joint Kinematics

There were a number of significant changes to joint-level gait kinematics due to the addition of an inertial disturbance on the shin. At the ankle, there was a reduction in peak plantarflexion during swing, and at all joints studied there was roughly 2% gait cycle temporal shift of most extrema towards the start of the gait cycle. This appeared to be the result of a slight, but significant temporal asymmetry in gait due to the increased mass of the shin. Kinematically at the knee there was a relatively large decrease in the peak knee flexion during swing of 7.5°. This reduction in knee flexion causes the ankle to dorsiflex roughly 8% sooner than normal in order to maintain necessary ground clearance. There was a reduction in swing flexion angular velocity at the hip and a reduction of knee angular velocity at toe-off, both of which significantly affect the peak swing flexion angle of the knee (Anderson et al. 2004). While the changes in many kinematic parameters are small, there was enough evidence to conclude that there was a kinematic reorganization in gait due to the inertial disturbance. There are some kinematic parameters which do not change with the added load. The peak loading response plantarflexion and terminal stance dorsiflexion of the ankle were not significantly different than normal. The knee angle at heel-strike, toe-off, and mid-stance peak flexion were also not significantly different than normal, in addition to the hip angle at toe-off and the peak hip extension.

5.2 Whole Body Gait Parameters

5.2.1 Motion of the Body Center of Mass

It was hypothesized, based on previous research, that the motion of the body center of mass had invariant tendencies when subject to inertial disturbance. Holt et al. (2003) found that when subjects wore a backpack with 40% body weight, the effective stiffness of the lower body increased so that the amplitude of the motion of the body center of mass orthogonal to the transverse plane was invariant to the inertial disturbance. The body center of mass was calculated as the loaded mean position of all body segments and added masses. In this thesis it was found that the motion of the adaptive loaded body center of mass orthogonal to the transverse and sagittal planes was largely not significantly different from normal. Only the amplitude of the BCOM motion orthogonal to the transverse plane was significantly greater than normal by 15%. The discrepancy between the results found in this thesis and the conclusions of Holt et al. (2003) may be due to the placement of the loads in each case. A backpack load is naturally close to the BCOM, and the motion away from the BCOM is limited. Whereas in this experiment with the load placed on the shin, the added mass is farther away from the BCOM and experiences a greater range of motion which may explain why there was a significant increase in the amplitude of the vertical excursions of the BCOM when the shin was loaded.

Orthogonal to the coronal plane there were significant deviations from normal for the adaptive loaded case of the RMS distance, distance amplitude, RMS velocity, and velocity amplitude of the body center of mass away from the linear fit. Most of the variance in the motion of the shank, where the additional mass was located, is perpendicular from the coronal plane, so this result is not surprising. Based on these results, there is enough evidence to reject the idea that the motion of the body center of mass is invariant when subjected to distal inertial disturbance. However, there is evidence to suggest that the motor control system makes some effort towards the goal of invariance of the body center of mass motion. In total 14 parameters defined by the motion of the body center of mass were compared across the various weighting conditions. A comparison of the adaptive loaded dataset with the normal indicated that 35.7% of parameters were significantly different, with an average change of 35.5%.

Comparing the non-adaptive loaded dataset to normal found that 85.7% of parameters were significantly different with an average deviation of 38.8%. The orthogonal coronal deviation of the body center of mass for the non-adaptive dataset was 187% greater than normal, compared to only 50% for the loaded dataset. These findings strongly suggest that the motor control system adjusts to the inertial disturbance in an attempt to keep the motion of the body center of mass invariant and the deviations small. This result is consistent with previous research which suggests that the body ambulates in a manner which keeps the oscillations of the body center of mass small (Fenn 1930, Hinrichs et al. 1987).

5.2.2   Gait Energetics

Normal walking involves the transfer of the body center of mass energy from gravitational potential to kinetic energy (Saibene 1990, Willems et al. 1995). The efficiency of this energy transfer, termed recovery, in normal walking as calculated in this thesis is on the order of 65%. When the mass was placed on the shin, the recovery dropped to 56%. However, the non-adaptive loaded dataset recovery dropped to nearly 44%. The reorganization of the walking pattern results in the increase of energy recovery from the non-adaptive loaded case to the true adaptive loaded case. While the percentage recovery was not invariant to distal inertial disturbance, there is sufficient evidence to suggest that one of the emergent properties of the reorganization of gait is an increase of efficiency. A total of four metrics of gait efficiency were calculated; without exception all efficiencies for the adaptive loaded case were lower than normal and all efficiencies for the adaptive loaded case were higher than the non-adaptive loaded case. In addition, a total of four metrics measuring RMS power and four metrics measuring total positive work were calculated. The RMS power and positive work metrics for the adaptive loaded case were consistently greater than normal at an average of 27% and 28% respectively. The non-adaptive loaded dataset had RMS power and positive work parameters that were 61% and 48% greater than normal respectively. Once again it was found that the reorganization of gait induces a direct reduction of the mechanical energetic costs of walking. From these results there was no such evidence to suggest a rejection of the hypotheses that the biologic performance

objective is to increase gait efficiency and reduce the energetic costs to move the body center of mass.

5.2.3 Whole Body Spin and Net External Torque

Analysis of the total angular momentum and total net external torque was generally inconclusive. Given the distance between the added mass and the body center of mass, and most of the motion of the added mass is in a tangential direction from the BCOM, it was expected that the adaptive loaded dataset should have significantly higher values of both spin and torque. Analyses revealed that the adaptive loaded dataset had larger magnitude extrema of both spin and net external torque as expected. A comparison of the adaptive loaded case and the non-adaptive loaded case the results was inconclusive; some peak parameters were higher for the adaptive loaded case and others for the non-adaptive loaded case, there was no consistent pattern of results. The sagittal RMS spin for the non-adaptive loaded dataset was higher than the adaptive loaded dataset; however the coronal RMS spin was lower for the non-adaptive loaded case than the adaptive loaded case. The transverse RMS spin was generally equivalent between the non-adaptive loaded and adaptive loaded datasets. Analysis of net external torque reveals similar results: The RMS torque was higher for the non-adaptive loaded dataset than for the adaptive loaded dataset in the sagittal plane, but the RMS torque for the non-adaptive loaded dataset was lower than for the adaptive loaded data in the transverse and coronal planes. In the sagittal plane, there was a consistent reduction in both spin and net external torque between the non-adaptive loaded dataset and the adaptive loaded dataset. Given that 80% of spin variance and 88% of net external torque variance was in the sagittal plane, when examining the data for deviations consistent with minimization of the performance criterion with respect to spin or net external torque, the sagittal plane should be of principle concern. The evidence suggests that, at least in the sagittal plane, an emergent property of the reorganization of gait is the reduction of net external torque and spin.

5.2.4   Angular Momentum Signal Cancellation

During normal walking there was an average of 95% signal cancellation in the sagittal plane of all body segments, and the adaptive loaded case has a significantly lower average signal cancellation of 85%. In symmetrical normal walking, the sagittal plane angular momentum of the right leg tends to offset that of the left leg (Popovic et al. 2004) leading to high average percentage signal cancellation. When a mass was added to the right leg however, there did not seem to be a large readjustment in the movement of the contralateral leg to offset the greater angular momentum of the affected leg. In the sagittal plane, the non-adaptive loaded test case had a mean angular momentum cancellation of 83% which was lower than the 85% of the adaptive loaded case. While the reorganization of gait yields an increase of signal cancellation on the order of 2% in the sagittal plane, there was a significantly greater increase in the transverse plane. The percentage signal cancellation of all body segments for normal walking was 89% in the transverse plane. The adaptive loaded trials had 85% transverse signal cancellation and the non-adaptive loaded dataset had 80% transverse signal cancellation for all body segments. In the transverse and sagittal planes, the two planes that have high percentages of signal cancellation, the reorganization of gait induces an increase in total body angular momentum signal cancellation.

5.3   Joint Kinetics

A comparison of the adaptive loaded versus normal dataset showed that there was a significant increase in a number of different kinetic parameters. The non-adaptive loaded dataset had a higher terminal swing torque at the knee and the hip, and a lower initial swing torque at the knee. While at first glance, these results seem to be inconsistent, it is important to keep in mind that examination of maxima during certain phases will not capture the total nature of the torque profile. Furthermore, the motor control system would most likely use as a performance criterion some function of the total sum of muscular effort. When the reaction torques were calculated for the loaded kinematics, but excluding the 5 kg mass in the calculations, all significant deviations from normal were reductions in joint torque or power. This result alone would suggest that walking in an asymmetrical manner could reduce joint torques. Given that subjects

without known pathologies generally walk in a symmetrical manner (Allard et al. 1996, Giakas & Baltzopoulus 1997, Sadeghi 2003), care should be taken in generalizing from the present results. However, the results in examination of the kinetics under various loading conditions are consistent with the hypothesis that the motor control system seeks to minimize some performance criterion function of joint torque and power.

5.4   Conclusions

The placement of a 5 kg mass distally on the shin did not induce dramatic kinematic changes in subjects' gait. There were significant changes in the motion at the hip, knee, and ankle; however most of these were generally small. Out of a total of 40 kinematic parameters, significant changes were found in 65% with the added load, and of those the change averaged 9.3%. A total of 27 kinetic parameters were compared for the adaptive loaded and normal case and 70% were significantly different by an average of 62%. From these results we can conclude that neither the kinematics nor the kinetics themselves are invariant to inertial disturbance. However, the absolute changes to kinematics in smaller.

From calculating the non-adaptive loaded dataset by placing a virtual 5 kg mass on the right shin, we can evaluate the effects of the adjustment in walking due to added mass. The changes in gait induce an increase in the percentage of body segment signal cancellation of linear and angular momentum. Furthermore, the true biological adaptive loaded case had higher gait efficiencies and smaller total amounts of positive work in all parameters that were significantly different than normal. This evidence suggests strongly that a main consideration of the motor control system is the reduction in the energetic costs of walking. There also appears to be a definite effort of the motor control system to reduce the peak torque and power on a joint level basis, which would be highly correlated with muscle activation levels and the metabolic rate associated with higher muscular activity. There is difficulty in this analysis in determining which changes in parameters are directly controlled, if any, and which changes are emergent. For example, it is possible that a minimization of the body center of mass work could also induce a reduction of joint torques and vice-versa, since these quantities are naturally highly correlated. It is evident that further work in this area is needed, to quantify how

the weighting of various parameters in the cost objective function would change the predicted gait pattern.

5.5   Future Work

Many of the gait parameters analyzed are naturally highly correlated, so it is difficult to specify the degree to which the motor control system controls these properties individually. A reduction in joint torques will induce a reduction in joint power for example. The next step in this process is to perform various spatiotemporal optimizations of the gait cycle for a reduced order model of the body. The first model should consist of a seven-link planar biped: feet, shins, thighs, and the head, arms, and torso (HAT) lumped as one segment. This model will only be useful for recreating behavior in the sagittal plane, so once again the scope is limited. If the planar model can reproduce biologically realistic gait patterns, a full three dimensional model could be built. It is a basic assumption in this future work that the performance criterion for walking is invariant to inertial disturbances. The cost function could be tuned upon both sets of data, or only on a portion of the data then used to predict the gait patterns for the untested case as a means for validation. A metric must be defined that will allow a performance based comparison of the simulated gait patterns, then the weighting of the terms in the cost function will be optimized themselves to maximize this biological realism performance metric. In this sense, two data points of normal morphology and loaded morphology would be used to fit the biologic cost function. Then this biologic cost function could be used to predict the optimal motion for a system with abiological morphology.

5.6   Summary

There exists a need for rapid online generation of gait patterns for the use in control of humanoid robotics and advanced prostheses. Kinematic trajectories can be generated by solving an optimization problem by minimizing a biologically inspired performance criterion. Reasonable biologic behavior has been generated by cost functionals based on jerk, joint torque, metabolic cost, mechanical energy, and

acceleration of the head (Marshall et al. 1989). Many of these cost functionals have been biologically inspired and their validity qualitatively analyzed by the degree to which they generate biologically realistic results. A different method was taken in this thesis; subjects were perturbed with an inertial disturbance and the deviations quantitatively calculated. Furthermore, by virtually placing a 5 kg mass on the shin when processing the kinematics for normal walking, a virtual reference dataset was created. This virtual non-adaptive reference dataset served as assumed "starting point" for the motor control system, and thus all deviations from this point were assumed to be the result of the biological optimization process. I hypothesized that the motor control system by minimizing the performance criterion will: keep the motion of the body center of mass invariant, increase gait efficiencies, decrease total work to move the body center of mass, and generally induce a reduction of joint torques. From the results presented in thesis, I conclude that the body center of mass is not invariant when a human is subject to inertial disturbance; however the motor control system makes some effort towards this regard. The non-adaptive loaded reference dataset had higher calculated total work and power requirements, and lower efficiencies. Therefore, it is my conclusion, that reducing the energetic costs of walking is a chief component in the biologic cost objective. Additionally, there appears to be a reduction in peak joint torques induced by the deviation in kinematics. The next step in this total process is to use the experimental gait data to fit biologic performance criteria on a reduced order model and quantitatively measure the biological cosmesis.

References

Abe, D., K. Yanagawa, and S. Niihata, 2004. Effects of load carriage, load position, and walking speed on energy cost of walking. Applied Ergonomics 35, 329-335

Allard, P., R. Lachance, R. Aissaoui, and M. Duhaime, 1996. Simultaneous bilateral 3-D able-bodied gait. Human Movement Science 15, 327-346

Anderson, F.C. and M.G. Pandy, 1999. A dynamic optimization solution for vertical jumping in three dimensions. Computer Methods in Biomechanics and Biomedical Engineering 2, 201-231

Anderson, F.C. and M.G. Pandy, 2001. Static and dynamic optimization solutions for gait are practically equivalent. J. Biomech. 34, 153-161.

Anderson, F.C., S.R. Goldberg, M.G. Pandy, and S.L. Delp, 2004. Contributions of muscle forces and toe-off kinematics to peak knee flexion during the swing phase of normal gait: and induced position analysis. J. Biomech. 37, 731-737

Bard, G. and H.J. Ralston, 1959. Measurement of energy expenditure during ambulation, with special reference to evaluation of assistive devices. Arch. Phys. Med. Rehabil. 40, 415-420

Becket, R. and K. Chang, 1968. An evaluation of the kinematics of gait by minimum energy. J. Biomech. 1, 147-159

Blaya, J., 2003. Force-Controllable Ankle Foot Orthosis (AFO) to Assist Drop Foot Gait. Master's Thesis. Cambridge, Massachusetts.

Bonnard, M. and J Pailhous, 1991. Intentional compensation for selective loading affecting human gait phases. Journal of Motor Behavior 23, 4-12

Chou, L.S., S.M. Song, and L.F. Draganich, 1995. Predicting the kinematics and kinetics of gait based on the optimum trajectory of the swing limb. J. Biomech. 28, 377-385

Chow, C.K. and D.H. Jacobson, 1971. Studies of human locomotion via optimal programming. Mathematical Biosciences 10, 239-306.

Crowe, A. and M.M. Samson, 1997. 3-D analysis of gait: the effects upon symmetry of carrying a load in one hand. Human Movement Science 16, 357-365

De Leva, P., 1996. Adjustments to Zatsiorsky-Seluyanov's segment inertia parameters. J. Biomech. 29, 1223-1230

DeVita, P., D. Hong, and J. Hamill, 1991. Effects of asymmetric load carrying on the biomechanics of walking. J. Biomech 24, 1119-1129

Donker, S., 2002. Flexibility of human walking: a study on interlimb coordination. Ph.D. Thesis. University of Groningen, Groningen, Netherlands.

Donn, J.M., D. Porter, and V.C. Roberts, 1989. The effect of footwear mass on the gait patterns of unilateral below-knee amputees. Prosthetics and Orthotics International 13, 140-144

Ehara, Y., H. Fujimoto, S. Miyazaky, M. Mochimaru, S. Tanaka, and S. Yamamoto, 1997. Comparison of the performance of 3-D camera systems II. Gait & Posture 5, 251-255

Fenn, W.O., 1930. Work against gravity and work due to velocity changes in running. American Journal of Physiology 93, 433-462

Ferris, D.P., K. Liang, and C.T. Farley, 1999. Runners adjust leg stiffness for their first step on a new running surface. J. Biomech 32, 787-794

Giakas, G. and V. Baltzopoulus, 1997. Time and frequency domain analysis of ground reaction forces during walking: an investigation of variability and symmetry. Gait & Posture 5, 189-197

Gitter, A., J. Czerniecki, and M. Meinders, 1997. Effect of prosthetic mass on swing phase work during above-knee amputee ambulation. Am. J. Phys. Med. Rehabil. 76, 114-121

Givoni, B. and R.F. Goldman, 1971. Predicting metabolic energy cost. Journal of Applied Physiology 30, 429-433

Godfrey, C.M., R. Brett, and A.T. Jousse, 1977. Foot mass effect on gait in the prosthetic limb. Arch. Phys. Med. Rehabil. 58, 268-269

Hale, S.A., 1990. Analysis of the swing phase dynamics and muscular effort of the above-knee amputee for varying prosthetic shank loads. Prosthetics and Orthotics International 14, 125-135

Hatze, H., 1976. The complete optimization of human motion. Mathematical Biosciences 28, 99-135

Hillery, S.C., E.S. Wallace, R. McIlhagger, and P. Watson, 1997. The effect of changing the inertia of a trans-tibial dynamic elastic response prosthesis on the kinematics and ground reaction force patterns. Prosthetics and Orthotics International 21, 114-123

Hinrichs, R.N., P.R. Cavanagh, and K.R. Williams, 1987. Upper extremity function in running. 1: Center of mass and propulsion considerations. International Journal of Sport Biomechanics 3, 222-241

Holt, K.G., J. Hamill, and R.O. Andres, 1990. The force-driven harmonic oscillator as a model for human locomotion. Human Movement Science 9, 55-68

Holt, K.G., R.C. Wagenaar, M.E. LaFiandra, M. Kubo, and J.P. Obusek, 2003. Increased musculoskeletal stiffness during load carriage at increasing walking speeds maintains constant vertical excursion of the body center of mass. J. Biomech 36, 465-471

Kamon, E., K.F. Metz, and K.B. Pandolf, 1973. Climbing and cycling with additional weights on the extremities. Journal of Applied Physiology 35, 367-370

Knapik, J., E. Harman, and K. Reynolds, 1996. Load carriage using packs: A review of physiological, biomechanical and medical aspects. Applied Ergonomics 27, 207-216

LaFiandra, M., K.G. Holt, R.C. Wagenaar, and J.P. Obusek, 2002. Transverse plane kinetics during treadmill walking with and without load. Clinical Biomechanics 17, 116-122

Lehmann, J.F., R. Price, R. Okumura, K. Questad, B.J. de Lateur, and A. Négretot, 1998. Mass and mass distribution of below-knee prostheses: Effect on gait efficacy and self-selected walking speed. Arch. Phys. Med. Rehabil. 79, 162-168

Lin-Chan, S.J., D.H. Nielsen, H.J. Yack, M-J Hsu, and D.G. Shurr, 2003. The effects of added prosthetic mass on physiologic responses and stride frequency during multiple speeds of walking in persons with transtibial amputation. Arch. Phys. Med. Rehabil. 84, 1865-1871

Mattes, S.J., P.E. Martin, and T.D. Royer, 2000. Walking symmetry and energy cost in persons with unilateral transtibial amputations: Matching prosthetic and intact limb inertial properties. Arch. Phys. Med. Rehabil. 81, 561-568

Marshall, R.N., G.A. Wood, and L.S. Jennings, 1989. Performance objectives in human movement: a review and application to the stance phase of normal walking. Human Movement Science 8, 571-594

Meikle, B., C. Boulias, T. Pauley, and M. Devlin, 2003. Does increased prosthetic weight affect gait speed and patient preference in dysvascular transfemoral amputees. Arch. Phys. Med. Rehabil. 84, 1657-1961

Miller, J.F., and B.A. Stamford, 1987. Intensity and energy cost of weighted walking vs. running for men and women. Journal of Applied Physiology 62, 1497-1501

Nubar, Y. and R. Contini, 1961. A minimum principle in biomechanics. Bulletin of Mathematical Biophysics 23, 377-391.

Perry, J., 1992. *Gait Analysis: Normal and Pathological Function*. SLACK Inc., New Jersey.

Popovic, M., A. Englehart, and H. Herr, 2004. Angular momentum primitives for human walking: Biomechanics and control. IEEE/RSJ International Conference on Intelligent Robots and Systems. Sendai, Japan

Sadeghi, H., 2003. Local or global asymmetry in gait of people without impairments. Gait & Posture 17, 197-204

Saibene, F., 1990. The mechanisms for minimizing energy expenditure in human locomotion. European Journal of Clinical Nutrition 44, 65-71

Siegel, K.L., T.M. Kepple, and S.J. Stanhope, 2004. Joint moment control of mechanical energy flow during normal gait. Gait & Posture 19, 69-75

Skinner, H.B. and R.L. Barrack, 1990. Ankle weighting effect on gait in able-bodied adults. Arch. Phys. Med. Rehabil. 71, 112-115

Soule, R.G. and R.F. Goldman, 1969. Energy cost of loads carried on the head, hands, or feet. Journal of Applied Physiology 27, 687-690

Sutherland, D.H., 1990. *The Development of Mature Walking*. Cambridge University Press, New York.

Tilley, A.R., 2001. *The Measure of Man and Woman: Human Factors in Design*. Wiley, New York.

Whittle, M.W., 1996. *Gait Analysis an introduction*. Reed Educational and Professional Publishing Ltd., Oxford.

Willems, P.A., G.A. Cavagna, and N.C. Heglund, 1995. External, internal and total work in human locomotion. Journal of Experimental Biology 198, 379-393

Wilcoxon, F., 1945. Individual comparisons by ranking methods. Biometrics Bulletin 1, 80-83

Winter, D.A., 1990. *Biomechanics and Motor Control of Human Movement*. Wiley-Interscience Publication, New York.

Winter, D.A., 1992. Foot trajectory in human gait: A precise and multifactorial motor control task. Physical Therapy 72, 45-56

Zatsiorsky, V., V. Seluyanov, and L. Chugunova, 1990. Methods of determining mass-inertial characteristics of human body segments. In *Contemporary Problems of Biomechanics*, 272-291. CRC Press, Massachusetts